学位申請論文

青井　真

Doctor thesis

Boundary Shape Waveform Inversion for Two-Dimensional Basin Structure using Array Data

by Shin AOI

Contents

Abstract

We propose a new method of waveform inversion of the underground structure to determine the shape of irregular basement of two dimensional basin structure, and examine the validity of this method by numerical experiments. It is well known that when seismic waves impinge on a basin structure, because of the reverberation of S waves in soft sediments, and the surface waves which are generated secondarily by the irregular structure such as the edge of a basin, we observe the ground motions of large amplitude and long duration. The waveforms observed on the surface are thus largely influenced by the basin structure, making the detailed knowledge of an underground structure very important.

In the sedimentary basin, since the impedance ratio is quite large between a hard basement with a high wave velocity and a soft sedimentary layer with a low wave velocity, we can consider that each of them consists approximately homogeneous elastic medium. Then, in the first part, we make a formulation of a boundary shape waveform inversion for a plane SH wave impinging on a two-layered structure. We discretize

the boundary shape and represent it by several parameters. The difference between the synthetic waveforms obtained by the use of the initial model constructed from a priori information and the data is caused by the difference between the assumed initial model and the true underground structure. We find out the boundary shape which explains the data best in the sense of the least square. Since this waveform inverse problem is essentially a non-linear problem, we use the linearized iterative method. We determine the correction value of parameters from the linearized equation, and use the model determined in this way as the initial model for the next iteration step. This iteration process is repeated until the residual converges. When the residual of the data becomes sufficiently small, we consider it as the ultimately estimated model. In order to show the validity of the present method, we carry out the numerical experiments with the synthetic waveform for a given target model as data. We can estimate the entire underground structure with waveforms from only a few observation stations on the surface, as long as we use as data not only the direct waves which contain the information concerning the un-

derground structure just underneath these observation stations but also the entire waveforms, including the surface waves generated secondarily by the irregular structure. The introduction of the hierarchical scheme, in which the parameters are increased gradually, enables a more stable computation within a shorter computation time. We also show that the method is robust and enables us to estimate the structure accurately even when there is a noise in the data or when there is an error in the given parameters.

In the second part, we extend this method to the so-called 2.5-D problem, that deals with 3-D wavefield for 2-D structure. This extension makes it possible to apply this inversion method to the case where the hypocenter is located in an azimuthally oblique direction in respect to the structure. We demonstrate through the examination of condition number of the linearized equations and the numerical experiments that the inversion analysis is more stable with three components than that with only one of them. Furthermore, we also show that for complex structures, certain parts of the structure are easier to estimate than others, and that

it depends on the direction from which the incident wave impinges. In such cases, we can estimate the entire structure with increased stability and accuracy by using simultaneously the data from incident waves from several directions.

Conclusively, in this study we carry out the new formulation for the boundary shape waveform inversion and successfully perform the numerical experiments. We generalize this method from SH problem to the 2.5-D problem to be applicable for practical cases of earth sciences, and also show its robustness by the numerical experiments for the cases where there is a noise in the data or error in the given parameters. This leads us to conclude that the method proposed here is applicable to the real data.

Acknowledgment

I am deeply grateful to Prof. Kojiro Irikura of Disaster Prevention Research Institute of Kyoto University who has been my supervisor during my doctor course, and provided me numerous discussions and seminars. A month and a half in Mexico with him was a very fruitful period in my research. I express my gratitude to Mr. Tomotaka Iwata of the same institute who gave me the research theme, provided me an experienced viewpoint and encouraged my research. I would also like to thank Prof. Yoshimasa Kobayashi of Aso Volcano Laboratory of Kyoto University, who was my supervisor during my master course. Thanks are also given to Dr. Koji Matsunami for his kind help for the observations.

I thank Prof. Sánchez-Sesma of UNAM, Dr. Hiroyuki Fujiwara, Dr. Hiroshi Takenaka and Dr. Hiroshi Kawase who taught me about numerical calculations including boundary integral method I am thankful to Mr. Yuzo Shinozaki of Faculty of Engineering of Kyoto University and Mr. Masanori Horike of Osaka Institute of Technology for their most helpful suggestions. I also appreciate the most helpful advice of Mr. Tomoki Tsutsui of Aso Volcano Laboratory of Kyoto University, Mr. Takao Kagawa of Geo-Research Institute, Osaka, and Mr. Sumio Sawada of Faculty of Engineering of Kyoto University.

I also thank Messrs Yasumaro Kakehi, Shinji Kawasaki, Hiroyuki Nakamura, Ken Hatayama, Arben Pitarka, Hiroo Nemoto, Jorge Aguirre, Susumu Inaba, Hiroshi Nakagawa, Ceser Moya, Ms. Midori Yamamoto, Haruko

Sekiguchi for their discussions and kind help.

The calculations presented in this paper were performed in part in the Supercomputer Laboratory, Institute for Chemical Research, Kyoto University.

Finally, I thank my parents who supported me fully in completing this research and let me continue my studies.

主論文 1

Part I

Waveform inversion for determining the boundary shape of a basin structure

ABSTRACT

We developed a method for estimating the boundary shape of a basin structure using seismograms observed on the surface. With this waveform inversion scheme, an accurate estimation is possible with data from a few surface stations, because seismic waves are affected not only by the local structure beneath the observation station but also by the entire basin structure. Numerical experiments were successfully carried out to determine the boundary shapes from observed surface records for a two-dimensional SH problem. For simplicity, only the boundary shape, that is thickness variations in the sedimental layer, was used as model parameters. This non-linear problem is solved iteratively. To avoid the instabilities resulting from inappropriate initial models or from a large number of parameters, a hierarchical method, in which the number of parameters are increased gradually, is developed. We also successfully performed the inversions when the given parameters contain some errors and when the data contain noise.

INTRODUCTION

When seismic waves impinge on a basin from below, the seismic waves observed on the surface of that basin are affected by the physical properties and boundary shape of the basin. Ground motions of large amplitude and long duration are considered to be caused by the reverberation of S waves in soft sediments, or to be surface waves generated secondarily at the basin's edges. In the 1985 Michoacan earthquake of M_s8.1, Mexico City was severely damaged, although it is located more than 400 km from the epicenter. The damage was concentrated in a soft sediment area, the so-called lake zone. Compared with records from a surface station on a hill zone (bedrock) only 5 km from a lake-zone station, the peak accelerations recorded in the latter zone was about five times larger and the duration was much longer (e.g., Beck and Hall, 1986). Many observations confirm the extraordinary effect of subsurface topography in other areas as well (e.g., Yamanaka et al., 1989).

Many methods have been proposed for the calculation of syn-

thetic waveforms in a laterally irregular structure: the Aki-Larner method (Aki and Larner, 1970), the finite-difference method (e.g., Boore, 1972), the finite-element method (e.g., Smith, 1975), and the boundary-element method (e.g., Sánchez-Sesma and Esquivel, 1979). Forward modeling performed with these methods has shown numerically that seismic waves of large amplitude and long duration occur (body waves amplified by soft sediments and surface waves generated secondarily at the edges of a basin) even for a simple body wave that impinges on the basin structure (e.g., Horike, 1987; Kawase and Aki, 1989). Furthermore, waveforms recorded on the surface have been shown to vary with the shape of the basin boundary (Bard and Bouchon, 1980).

The purpose of our study was to estimate the boundary shape of an underground structure by waveform inversion using seismograms observed on the surface. This is a type of domain/boundary inversion (Kubo, 1992), a method for estimating the boundary shapes of several regions regarded as homogeneous. The inversion using the shape of the boundary as the model parameters has already been studied in the mechanical engineering. For exam-

ple, there are some studies for detecting the shapes and locations of cracks from the static, or occasionally dynamic, responses of mass (e.g., Nishimura and Kobayashi, 1991, Tanaka and Yamagiwa, 1988). Another example is a study of the shape optimal problem (Barone and Caulk, 1982). In exploration geophysics, there have also been some attempts to estimate the boundary shape of the velocity discontinuity by applying the refraction (White, 1989) or the reflection method (Nowack and Braile 1993) for the seismic wave. However, the resolution of the refraction method is low since it uses only a limited information at the arrival time. This does not fully utilize the information coming from the data. In the case of the reflection method, the data acquisition takes a long time since it spatially requires many observation data. Therefore, we will propose a method to estimate the underground structure by using the entire waveforms from earthquakes recorded at the small numbers of surface stations, including not only the direct waves but also the later phases.

In many cases of realistic geological structure, both sediment and basement layers are considered to be roughly homogeneous in

the light of the high impedance ratio between them. Therefore, we assume that the basin structure discussed here is composed of two homogeneous layers divided by an irregular interface. We also assume that average velocities for the layers are known, and seek to estimate the boundary shape. The boundary shape can be estimated directly from observed seismograms, using a small number of parameters to describe the boundary. We have assumed a two-dimensional problem and formulated a boundary shape waveform inversion for a plane SH wave impinging on a two-layered structure, and examined the validity of this inversion using numerical experiments. Inversions were performed for a given S wave velocity and density for each layer and a given basin width. Since this is a non-linear inverse problem, the solution is obtained by the linearized iterative method. To avoid computational instabilities (divergence or oscillation of the parameters) resulting from an inappropriate initial model or from a large number of parameters when the inversion is performed, the hierarchical method, in which the parameters are increased gradually, is proposed. We also performed the inversions when the assumed velocities are incorrect and when the data

contain noise.

EFFECTS OF THE BASIN STRUCTURE ON SEISMIC WAVES RECORDED ON THE SURFACE

To evaluate seismic waveforms on the surface when a plane SH wave impinges on a basin structure, we consider a basin structure model that consists of a homogeneous, isotropic, elastic layer underlain by a homogeneous, isotropic, elastic half space. A two-dimensional (2-D) SH problem is assumed and the seismograms on the surface, when a plane SH wave impinges from the half space, are calculated using the boundary element method (Sánchez-Sesma et al., 1993).

We investigated a basin structure, Model 0 in Fig. 1 and Tables 1 and 2. Its width is 10 km, β_1 =1km/s, β_2=2.5km/s, $\rho_1 = \rho_2$, and its maximum depth 1 km. The boundary shape is a parabola (β represents the S wave velocity and ρ the density, and the suffix depicts the layer number.). A plane SH Ricker wavelet (Ricker, 1977) with the characteristic frequency of f_c,

$$u(t) = (2\pi^2 f_c^2 t^2 - 1)\exp(-\pi^2 f_c^2 t^2), \qquad (1)$$

where $u(t)$ is displacement, was used as the incident wave. Seismograms on the surface when a Ricker wavelet with the characteristic period of 2 seconds impinges on Model 0 vertically from below are shown in Fig. 2a. For simplicity, attenuation of the seismic wave in the propagation media is not considered in this investigation. Although the incident wave is a simple Ricker wavelet, its later phases are as equally prominent as direct waves. These later phases are surface waves generated secondarily at the edges of the basin(e.g., Horike, 1987).

We performed an one-dimensional (1-D) analysis to learn the influences of lateral heterogeneity on seismogram on the surface. We assumed a horizontally-homogeneous, stratified structure based on the local structure beneath each surface station, and calculated the surface waveform generated by a vertically incident SH wave from below by using the Haskell's method (Haskell, 1953). We call this an 1-D analysis in the sense that it evaluates only the effect of the vertical heterogeneity. The synthetic waveform obtained by this 1-D analysis (Fig. 2b) is composed of a direct body wave and small reverberations within the surface layer. The remarkable surface

waves seen as later phases in the 2-D analysis are not reproduced in the 1-D analysis. Hence, when the structure varies laterally, the observed waveform on the surface is influenced not only by the local structure but by the entire basin structure. This suggests that if we use the full waveform, including the later phases, we may be able to estimate the entire structure for a two-dimensional problem using data from only a small number of stations. In contrast, if only the arrival time and direct wave are used, records from numerous stations are required to estimate the underground structure. The incident wave used in our numerical experiments therefore is a Ricker wavelet with a characteristic period of 2 to 3 seconds, for which the surface wave generated secondarily becomes prominent for the basin structure model assumed.

FORMULATION OF THE INVERSION

Basis functions and model parameters for the boundary shape

We require a means of representing the boundary shape using a limited number of parameters. It is convenient if the boundary shape $\zeta(x)$ is represented by the basis function $c_k(x)$ and the real

number parameter p_k as

$$\zeta(x) = \sum_k p_k \times c_k(x). \tag{2}$$

We therefore introduce the function system $\{c_k(x)|k = 1, 2, \cdots, K\}$,

$$c_k(x) = \begin{cases} 1/2 + 1/2\cos\{\pi/\Delta(x - x_k)\} & \text{if } x_{k-1} \leq x \leq x_{k+1} \\ 0 & \text{otherwise.} \end{cases} \tag{3}$$

The basin is located in the range of $-L < x < L$, and has a width of $2L$. The boundary is divided equally into $K+1$ parts with $K+2$ nodes (an interval $\Delta = 2L/(K+1)$). The first and last nodes being excluded, these K nodes are numbered from 1 to K. The x coordinate of the kth is denoted by x_k. Examples of the spatial distribution of the function system $c_k(x)$ for $K = 9$ are shown in Fig. 3. The solid line represents $c_k(x)$ for k=4. The boundary shape to be estimated, ζ, is denoted with this function system as

$$\zeta(x) = \zeta^0(x) + \sum_{k=1}^{K} p_k \times c_k(x) \tag{4}$$

where $\zeta^0(x)$ denotes the shape of the initial model. The parameter p_k physically represents the difference in depth between the target and initial models at x_k, $\zeta(x_k) - \zeta^0(x_k)$. The function system $c_k(x)$

interpolates the p_k's, giving the boundary depth at all discretized points.

Formulation of the inversion

The observation equation is

$$u(x_m, t_n; \boldsymbol{p}) = \tilde{u}_{mn} \qquad \text{(for all } m, n\text{)}. \tag{5}$$

The left side, $u(x_m, t_n; \boldsymbol{p})$, is a synthetic waveform at the m-th position, x_m, and the n-th sampling time, t_n, for the vector of the model parameters $\boldsymbol{p}$ ($\boldsymbol{p} = (p_1, p_2, \cdots, p_K)$). The right side, $\tilde{u}_{mn}$, is the observed waveform (given) at x_m and t_n. The vector parameter $\boldsymbol{p}$ is determined to satisfy the equation (5) in a least squares sense.

As this is a non-linear inverse problem, the solution is obtained by the linearized iterative method. A Taylor series expansion is performed on the left side of the equation (5) about the parameter $\boldsymbol{p}^0$ where $\boldsymbol{p}^0$ is the vector of the model parameters for the initial $\zeta^0(x)$. By omitting the higher order terms, this equation is linearized as

$$u(x_m, t_n; \boldsymbol{p}^0) + \sum_{k=1}^{K} \left. \frac{\partial u}{\partial p_k} \right|_{\boldsymbol{p}=\boldsymbol{p}^0} \delta p_k \simeq \tilde{u}_{mn}. \tag{6}$$

Because the differential seismogram $\partial u / \partial p_k$ cannot be obtained analytically, we replace it with a finite-difference approximation. Ap-

proximating equation (6) with finite-differences, we obtain

$$\sum_{k=1}^{K} \frac{u(x_m, t_n; \boldsymbol{p}^0 + \Delta \boldsymbol{p}_k) - u(x_m, t_n; \boldsymbol{p}^0)}{\Delta p_k} \delta p_k \simeq \tilde{u}_{mn} - u(x_m, t_n; \boldsymbol{p}^0), \tag{7}$$

where Δp_k is an appropriate positive number, and $\Delta \boldsymbol{p}_k = (0, \cdots 0, \Delta p_k, 0, \cdots, 0)$. Equation (7) is a set of simultaneous linear equations whose coefficient matrix is non-square. We use the singular value decomposition method to solve this equation (e.g., Aki and Richards, 1980, Nakagawa and Oyanagi, 1982).

In the inversion process described, the correction value for each parameter is determined. Using this value, we construct the starting model for the next iteration. The square sum, $\sum_{m,n}(\tilde{u}_{mn} - u(\boldsymbol{p}))^2$, of the residuals between the data and synthetic seismograms is used to check the degree of fit of the models. The solution that converges by the use of this linearized iterative method is considered the best model when the residuals are sufficiently small.

To perform a non-linear inversion with an iterative method, an appropriate initial model which consists of a priori information is necessary. This is a problem that we have to face inevitably.

and without enough a priori information, the inversion cannot be performed. However, in many cases, we have some information of the underground structure given by the borehole logs and gravity exploration, seismic exploration such as reflection method and refraction method. These pieces of information often enable us to construct an appropriate initial model, with which we can estimate a basin structure with seismic data.

Differential seismograms

When inversion of a boundary shape is performed using seismograms on the surface, the coefficient matrix of the linearized observation equation $\sum \partial u/\partial p_k \quad \delta p_k \simeq \tilde{u} - u(\boldsymbol{p}^0)$ is required. As stated earlier, $\partial u/\partial p_k$, the differential seismogram, is replaced by the finite difference $\Delta u/\Delta p_k$ in our method. This represents a sensitivity of a change in the waveform that corresponds to the change of the k-th model parameter p_k.

The case discussed here has nine model parameters (K =9). Fig. 4 shows the time and space distributions of the differential seismograms that correspond to the waveforms in Fig. 2a; the differ-

ential coefficient $\Delta u/\Delta p_k (k = 1 \sim 5)$ corresponds to the coefficient of $\delta p_1 \sim \delta p_5$. These differential seismograms are calculated with Δp_k =5×10^{-3}km; i.e., $\Delta p_k/L = 10^{-3}$, since L = 5km. This is considered to be a good approximation of $\partial u/\partial p_k$ because the value of Δp_k is sufficiently small compared with the width of the basin and the maximum depth (1 km). Moreover, the finite-difference value, $\Delta u/\Delta p_k$, is almost constant in the range of $\Delta p_k/L = 10^{-2} \sim 10^{-4}$. Fig. 4 indicates that lateral change in the layer depth influences not only the direct waves above but also secondarily-generated surface waves of the seismograms at all the surface stations. In addition, the change in depth near the edge of the basin has a greater effect on the surface seismograms than does the change in depth in the central part of the basin (e.g., compare Figs. 4a and 4e). The fact that the time and space distributions of $\Delta u/\Delta p_k$ totally differ depending on k suggests the possibility that we can invert the model parameters with sufficient resolution.

The differential coefficient $\Delta u/\Delta p_k$ is obtained by repeated computation of synthetic waveforms by forward modeling for many perturbed structures. When the boundary element method is used,

the most significant part of the computation consists of obtaining the Green's functions. Computation of the Green's functions is needed again only for those corresponding to the perturbed parts of the structures. The computation time needed for the inversion therefore can be greatly reduced because the same process is not repeated when local parameters are used.

HIERARCHICAL SCHEME OF INVERSION

When performing the inversion, computation becomes unstable (it means that parameters diverge or oscillate) if the given initial model is not appropriate or the number of parameters is too large. In such cases, a hierarchical scheme of inversion can improve the unstable computation. Though it is unnecessary to use the hierarchical method when an initial model is known to be appropriate, the use of this method is not harmful, which just requires more steps in the inversion. In all other cases, this method is useful in stabilizing the computation.

Appropriate initial model

A boundary shape can be estimated even from a few surface

stations when the inversion is performed with an appropriate initial model, as described in detail in the next section. An "appropriate" initial model here means that $\Delta\zeta_{max}$ is small enough compared with ζ_{max},

$$\Delta\zeta_{max} = \max_x |\zeta(x) - \zeta^0(x)|,$$

where $\zeta^0(x)$ and $\zeta(x)$ respectively are the depths of the initial and target models, and ζ_{max} the maximum depth of the sediment. Obviously, to select an appropriate initial model, one must incorporate all available a priori information about the basin.

In solving this kind of non-linear inverse problem, use of an inappropriate initial model leads to divergence or oscillation of the parameters in the early steps of iteration, and this unstable computation makes it difficult to extract the information contained in the data.

Hierarchical scheme

Since the inversion tends to be unstable when there are many parameters, we introduced a hierarchical scheme (e.g., Kubo et al., 1988). This is a scheme to perform a stable inversion without losing

the resolution of the data: First, inversion is performed iteratively with a small number of parameters until the residuals converge, then the number of parameters is increased. For each increase in the number of parameters, additional iterations are made until the residuals again converge. Eventually the residuals stop decreasing, in spite of the increase in the number of parameters, when the number of parameters required to reproduce the target model is reached. The minimum number of parameters required to match the observation can be estimated roughly in this way.

NUMERICAL TESTS OF INVERSION METHOD

In our numerical experiments, we use waveforms synthesized from a target model as pseudo-observed data in order to show the usefulness of boundary shape inversion.

Models A and B in Fig. 1 and Table 1 are the target models. The physical constants of each layer in both models are listed in Table 2. Our data consist of the synthesized waveforms taken from several stations on the surface within the basin, computed assuming an incident plane SH wave with a Ricker wavelet time function.

The S-wave velocity and density for each layer, the width of the basin, and the angle and pulse-shape of the incident wave, assumed to be given without error, are given as a priori information. The case in which there are errors in these parameters is discussed later. For simplicity, the attenuation in propagation is not considered in this study, and the Q values for both layers are given as infinite. Otherwise, the Q values could be parameters to be estimated, although perhaps not uniquely. We used Model 0 as the initial model, as described in Fig. 1 and Tables 1 and 2.

Case A: Model A as the Target Model

The solid lines in Fig. 5 show the waveforms synthesized for three surface stations, using a Ricker wavelet with a characteristic period of three seconds impinging on Model A vertically from below. The data length is 8.7 seconds, from -1.9 to 6.8 seconds (sampling rate is 12.8Hz). The broken lines show the waveforms synthesized from the same incident wave that impinges on the initial model.

These waveforms were used as pseudo-data in the inversion with nine model parameters (K =9). The estimated models and

the residuals of each iteration step are shown respectively in Figs. 6 and 7. The residuals are normalized by that of the initial model. The residual decreases until the fourth iteration, becoming almost constant thereafter. The target model is estimated exceptionally well by the fourth iteration.

Thus, under ideal conditions, the shape of an entire structure can be estimated with data from only a few surface stations when the full waveforms, including the later phases, are used.

Case B: Model B as the Target Model

In this case, our target is Model B, and the initial model (Model 0) is not as close to the target model as it was in Case A, therefore, the hierarchical scheme is used. The basin of the target model has a smooth, lateral gradient in thickness, which increases to a maximum depth of 1.25 km, and truncates sharply near the right side of the model. The solid lines in Fig. 8 show waveforms synthesized for four surface stations using a Ricker wavelet with a characteristic period of three seconds impinging on Model B at the incident angle of 15 degrees to the left of the vertical line. The

data length is 16.4 seconds, from −1.9 to 14.5 seconds (sampling rate, 12.8Hz). The broken lines show the waveforms synthesized from the same incident wave that impinges on the initial model, Model 0. The waveforms shown by the solid and broken lines differ markedly. This indicates that the initial (Model 0) and target (Model B) models are not likely to be close.

Using these waveforms, we first performed the inversion with four parameters (K =4). The residual of each iteration step is shown in Fig. 9. The residual decreases until the fourth iteration, becoming almost constant thereafter. After the fourth iteration, the number of model parameters are increased from four to eight, after the eighth iteration to 12, and after the tenth to 16. As the parameters are increased by four from four to 12, the residuals decrease; yet, there is no further decrease when the parameters are increased to 16. This means that the data can be explained by a model with 12 parameters.

In each step of the hierarchical inversion the estimated model is compared with the target model (Fig. 10). Even with four parameters, the left half of the structure is well estimated (Fig. 10a):

the right half is not so well estimated because these four parameters cannot express the steep edge of Model B. An increase of number of the parameters to eight improves the estimation of the right side (Fig. 10b). With 12 parameters, the entire target model, including the right side, is estimated almost perfectly (Fig. 10c). In this case, 12 parameters sufficiently reproduce the model, which is consistent with earlier results for the convergence of residuals.

We conclude that when the hierarchical scheme is used, larger range of model parameters can be used for the initial model.

FURTHER TESTS WITH NOISE AND WITH ERRORS

Numerical experiments showed that the entire boundary shape can be estimated with noise-free data from only a small number of surface stations when the full waveforms including the later phases are used and when there are no errors in the initial velocity assumptions. Here, we discuss the effects of two types of errors (noise contained in the data and errors in the given parameters: the assumed velocity and incident angle) on inversion results.

Effects of noise in the data

Inversion is performed with data to which Gaussian noise has been added artificially in order to examine the effects of noise. The data were a wave field generated by a Ricker wavelet that has power in a very narrow band in the frequency domain. Therefore, Gaussian noise of zero mean and normal distribution is band-pass-filtered in the bandwidths two to five seconds, and then added to the data to include noise.

The target model, Model C, is shown in Fig. 1 and Tables 1 and 2. The broken line in Fig. 11 shows waveforms (without noise) synthesized from a Ricker wavelet with a characteristic period of 3 seconds, impinging vertically on Model C from below. The data constructed by adding noise to these waveforms are shown by the solid line in the same figure. Fig. 12a and b respectively show the waveforms at the center of the basin in the time and frequency domains. When the noise ratio is defined as $\sum|\text{noise}|/\sum|\text{data}|$ in the frequency domain, the noise ratio for the data in Fig. 11 is approximately 12%.

Results of the inversion are shown in Fig. 13; Model 0 was used as the initial model. The model is successfully estimated when

K =4 and K =8. The fact that the model can also be estimated with data containing noise reveals the significant potential of this method for dealing with real data. But, for a large number of parameters, such as K =12, small fluctuations that do not exist in the target model appear in the estimated model. These fluctuations occur because the number of parameters was increased beyond the amount of information contained in the data. The appropriate number of parameters therefore must be determined from the S/N ratio. The hierarchical inversion approach is ideally suited to select an appropriately parameterized model. Statistical tests, such as the Akaike information criterion (AIC: e.g., Nakagawa and Oyanagi, 1982), or the Akaike Bayesian Information Criterion (ABIC) could be used to select an appropriate number of model parameters.

Errors in given parameters

In the numerical tests discussed above, we assumed that parameters such as the S-wave velocity, density, and incident angle are known, except for the parameters of boundary shape. Actually such given parameters contain certain errors. Therefore, we

examined the effects on the inversion results by an error in S wave velocity and by an error in incident angle.

In the first example, the S wave velocity of the first layer is given as 5% faster than the true value. The data used for the inversion are the synthetic waveforms generated by a Ricker wavelet with a characteristic period of 3 seconds impinging vertically on Model C from below (Fig. 14). The same Model 0 was used as the initial model, except for $\beta_1 = 1.05$km/s. As shown in Fig. 15, the results closely reflect the true structure, but it is estimated to be about 10% deeper than the target structure. Since a trade-off exists between velocity and depth (Ammon et al., 1990), it is difficult to determine the absolute value of seismic wave velocity and the depth of the structure simultaneously in most seismic exploration methods, although there are some attempts to separate them (Olsen, 1989). The estimation of a deeper structure when an erroneously fast seismic wave velocity is assumed is therefore expected.

The second example is for an error in the incident angle. The data obtained from Model C are used, and the inversion was performed with Model 0 as the initial model. The given incident angle

is vertical, whereas the true incident angle is 5 degrees to the left. The results of inversion shown in Fig. 16 closely reflect the true structure, but the left half of the inverted boundary shape is estimated to be shallower and the right half deeper than the target. This is due to the phase shifts created by the error in the assumed incident angle: On the left side of the basin, the phases shift later than the true ones, whereas the phases shift earlier on the right side.

Although the noise contained in the data and the errors in the given parameters affect the estimations, our tests suggest that the models can be roughly estimated as long as the noise in the records used in the inversion is less than 15%, and the errors of S wave velocity and the incident angle are respectively within 5% and 5 degrees.

DISCUSSION

A question of extending this method to 3-D structures remains, since we cannot actually expect an ideal 2-D structure though 2-D SH problem was assumed for this study. Nevertheless, the

wavefields in some basin structures were well explained by the 2-D forward modeling (e.g., Yamanaka et al., 1989, 1992). In these cases, the 2-D problems are significant for realistic applications. Moreover, the formulation in the basic 2-D problems is useful as the first step, which can then be extended to invert fully 3-D structures.

When the effects of 3-D structure are strong, 2-D inversion will become insufficient. Therefore, we must also discuss the possibility of extending the method to 3-D inverse problems. The rapid progress in computers has recently made it possible to solve the 3-D problems. However, this does not imply that the 3-D inverse problems, especially the non-linear inverse problems, can be solved immediately, for the following reasons: First of all, in order to perform an inversion, the forward problems have to be solved repeatedly, which takes a long time; Secondly, the parameters to be estimated in a 3-D inverse problem are increased by square compared with those in a 2-D inverse problem; Moreover, we face a difficulty in obtaining data from many surface stations to cover a target area. The method proposed in this study will have certain advantages

over other conventional methods when it becomes possible to solve 3-D forward problems within a reasonable computation time and to challenge the 3-D inverse problems. First of all, the use of the full waveform enables us to perform the inversion with data from less stations, when compared to the methods which employ only the direct waves. Moreover, compared with a conventional method such as the tomography, in which the parameters have to be estimated at all grid points, the number of parameters to be estimated is much less in our method. By extending equation (4), the representation of the boundary shape in 2-D problem, in a 3-D problem, it is represented as

$$\zeta(x,y) = \zeta^0(x,y) + \sum_{i,j} p_{ij} \times c_{ij}(x,y) \tag{8}$$

where p_{ij} is a parameter that represents the boundary shape and

$$c_{ij}(x,y) = c_i(x)c_j(y). \tag{9}$$

The right side of this equation is a basis function defined in equation (3).

One difficulty of extending our inversion method to the 3-D problem, and also to the 2-D P-SV problem, is the evaluation of

the incident wavefield. While a simple SH plane wave is assumed in this study, the incident wavefield in reality consists of P-wave, S-waves and surface waves, which makes it necessary to separate them. One possible solution to evade this problem would be the introduction of a point source. In any case, the high possibility of extending our inversion method to the 2-D P-SV problems and the 3-D problems has to be emphasized.

CONCLUSIONS

We developed a method for estimating the boundary shape of a basin structure using waveform inversion. We formulated a boundary shape waveform inversion for the case of a plane SH wave impinging on a two-layered structure and examined the validity of that inversion with numerical experiments.

The boundary shape of the entire basin could be estimated almost perfectly from records taken from only a small number of surface stations by using the full waveform, including the later phases, when an appropriate initial model is given. When the value of $\Delta\zeta_{max}$ is large, which means that the initial model is inappropriate,

the computation becomes unstable. In such cases, stable computation may be obtained by a hierarchical scheme of inversion which consists of gradually increasing the number of model parameters. To check the effects of errors on the inversion, we investigated cases of data containing noise and cases of given parameters containing errors. Although errors do affect the inversion, the structure can be estimated roughly as long as the errors are not very large (noise in the records less than 15% and the errors of S wave velocity and the incident angle respectively within 5% and 5 degrees).

Our simple assumption of a two-dimensional, two-layered structure and an SH wave field does not stem from any essential difficulty. The method described therefore can be expanded to more general problems such as the P-SV wave field.

Acknowledgments

We thank Hiroshi Kawase, Hiroshi Takenaka and Hiroyuki Fujiwara for their most helpful suggestions. We are also grateful for the discussion and useful advice provided by Yoshimasa Kobayashi, Shoichi Kobayashi, Masanori Horike, and Yuzo Shinozaki. We acknowledge the critical reviewing of Charles Ammon, John Cassidy and an anonymous referee.

References

Aki, K. and K. L. Larner (1970). Surface motion of a layered medium having an irregular interface due to incident plane SH waves, *J. Geophys. Res.* **75**, 933-954.

Aki, K. and P. G. Richards (1980). *Quantitative Seismology: Theory and Methods,* W. H. Freeman and Co., San Francisco.

Ammon, C. J., G. E. Randall and G. Zandt (1990). On the nonuniqueness of receiver function inversions, *J. Geophys. Res.* **95**, 15303-15318.

Bard, P Y. and M. Bouchon (1980). The seismic response of sediment-filled valleys, Part 1: The case of incident SH waves, *Bull. Seism. Soc. Am.* **70**, 1263-1286.

Barone, M. R. and D. A. Caulk (1982). Optimal arrangement of holes in a two-dimensional heat conductor by a special boundary integral method, *Int. J. Num. Meth. Eng.* **18**, 675-685.

Beck, J. L. and J. F Hall (1986). Factors contributing to the catastrophe in Mexico City during the earthquake of September 19 1985, *Geophys. Res. Lett.* **13**, 593-596.

Boore, D. M. (1972). Finite difference methods for seismic wave propagation in heterogeneous materials, in *Methods in Computational Physics*, by B.

A. Bolt(Editor), Vol. 11, Academic Press, New York.

HASKELL, N. A. (1953). The dispersion of surface waves in multilayered media, *Bull. Seism. Soc. Am.* **43**, 17-34.

HORIKE, M. (1987). Extension of the Aki and Larner method to absorbing media with plural curved interfaces and several characteristics of a seismic response on a sedimentary basin, *Zisin Second series, (J. Seism. Soc. Japan)* , **40**, 247-259 (in Japanese with English abstract).

KAWASE, H. and K. AKI (1989). A study on the response of a soft basin for incident S, P, and Rayleigh waves with special reference to the long duration observed in Mexico City, *Bull. Seism. Soc. Am.* **79**, 1361-1382.

KUBO, S., T. SAKAGAMI, K. OHJI, T. HASHIMOTO and Y. MATSUMURO (1988). Quantitative Measurement of Three-Dimensional Surface Cracks by the Electric Potential CT Method, *J. Mech. Soc. Japan* A-**54**-498, 218-225 (in Japanese with English abstract).

KUBO, S. (1992). *Inverse Problems,* Baifukan, Tokyo (in Japanese).

NAKAGAWA, T. and Y OYANAGI (1982). *Experimental Data Analysis by the Least-Squares Method,* Univ. of Tokyo Press, Tokyo (in Japanese).

NISHIMURA, N. and S. KOBAYASHI (1991). A boundary integral equation method for an inverse problem related to crack detection, *Int. J. Num. Meth. Eng.* **32**, 1371-1387.

NOWACK, R. L. and L. W BRAILE (1993). Refraction and wide-angle reflection tomography: theory and results, *Seismic Tomography: Theory and Practice*, 733-763.

OLSEN, K. B. (1989). A stable and flexible procedure for the inverse modelling of seismic first arrivals, *Geophys. Prospecting* **37**, 455-465.

RICKER, N. H. (1977). Transient waves in visco-elastic media, Amsterdam.

SÁNCHEZ-SESMA, F J. and J. A. ESQUIVEL (1979). Ground motion on alluvial valleys under incident plane SH waves, *Bull. Seism. Soc. Am.* **69**, 1107-1120.

SÁNCHEZ-SESMA, F J., J. RAMOSE-MARTÍNEZ and M. CAMPILLO (1993). An indirect boundary element method applied to simulate the seismic response of alluvial valleys for incident P, S and Rayleigh waves, *Earthq. Eng. and Struct. Dynamics* , **22**, 279-295.

SMITH, W D. (1975). The application of finite element analysis to body wave propagation problems, *Geophys. J. Roy. Astr. Soc.* **42**, 747-768.

TANAKA, M. and K. YAMAGIWA (1988). Application of boundary element method to some inverse problems in elastodynamics, *J. Mech. Soc. Japan* A-**54**-501, 1054-1060 (in Japanese with English abstract).

WHITE, D. J. (1989). Two-dimensional seismic refraction tomography, *Geophys. J.* **97**, 223-245.

YAMANAKA, H., K. SEO and T. SAMANO (1989). Effects of sedimentary layers on surface-wave propagation, *Bull. Seism. Soc. Am.* **79**, 631-644.

YAMANAKA, H., K. SEO and T. SAMANO (1992). Analysis and numerical modeling of surface-wave propagation in a sedimentary basin, *J. Phys. Earth* **40**, 57-71.

Tables

Table 1. Maximum depths and shapes of the structure models.

	Shape	max. Depth
Model 0	parabola	1.00km
Model A	trapezoid	0.75Km
Model B	non-symmetrical parabola	1.00km
Model C	parabola	1.25km
width of basin	10km	

Table 2.

Table 2. Physical parameters of the structure models.

	First layer	Second layer
S wave velocity β	1.0km/s	2.5km/s
Q-value	∞	∞
density ρ	$\rho_1 = \rho_2$	

Figure Captions

FIG. 1. Basin structures of Models 0, A, B and C. The shear-wave velocities β_1 and β_2 are respectively 1.0km/s and 2.5km/s and the density ρ_1 is given as equal to ρ_2 for these four models.

FIG. 2. Synthetic seismograms at ground surface for Model 0 for a Ricker wavelet with a characteristic period of two seconds (vertical incidence). The underground structure is shown on the right of the seismogram. (a): the 2-D analysis (BEM) and (b): the 1-D analysis (*Haskell* method). Although there is similarity in the direct wave part in both figures, the surface waves are predominant only in the 2-D case.

FIG. 3. Examples of the space distribution of the weight function system $c_k(x)$ when K=9. Solid line shows the example of $c_k(x)$ for k=4.

FIG. 4. Differential seismograms $\Delta u/\Delta p_k$ of Model 0 for $K = 9$. (a) through (e) corresponds to k =1 through 5.

FIG. 5. Seismograms recorded at three surface stations for the target (Model A) and initial (Model 0) models shown respectively by solid and broken lines. They were produced by a Ricker wavelet with a characteristic period of two seconds impinging on the models vertically from below. The incident wave is shown in the bottom trace.

FIG. 6. Results of the inversion. The initial (Model 0) and target (Model A) models, and estimated models obtained by the first to the fourth iterations are shown respectively by (a) through (d).

FIG. 7. Change of the square sum of the residuals after each iteration for the inversion in Case A. The residuals are normalized by that of the initial model. They decrease monotonically, and converge at the third iteration.

FIG. 8. Seismograms for the target (Model B) and initial (Model 0) models shown respectively by solid and broken lines. They were produced by a Ricker wavelet with a characteristic period of three seconds impinging on the models from below at an angle of 15° to the left.

FIG. 9. Change in the square sum of the residuals after each iteration in the inversion for Case B. The residuals are normalized by that of the initial model. In the hierarchical scheme, the number of parameters is increased by four each time the residuals converge.

FIG. 10. Results of the inversion. (a) through (d), respectively, show the initial (Model 0), target (Model B), and estimated models at each step of the hierarchy.

FIG. 11. Data used to examine the effects of noise on inversion. Broken line: data without noise. Solid line: data with Gaussian noise with zero mean and normal distribution bandpass-filtered between two and five seconds.

FIG. 12. Data with (broken line) and without (solid line) noise at the center of the basin (x=0) in the (a)time and (b)frequency domains.

FIG. 13. Results of inversion with data containing noise. The correct model can be estimated with data containing noise (a,b), but undesirable fluctuation occurs when too many parameters are introduced (c).

FIG. 14. Seismograms recorded at four surface stations for the target (Model C) and initial (Model 0) models shown respectively by solid and broken lines. They were produced by a Ricker wavelet with a characteristic period of three seconds impinging on the models vertically from below.

FIG. 15. Results of inversion with Model 0 as the initial model but with β_1 =1.05km/s. The estimated model closely reflects the target structure, but is estimated as being deeper than the target.

FIG. 16. Results of inversion with Model 0 as the initial model when the given incident angle is vertical, whereas the true incident angle is 5° to the left. The estimated structure closely reflects the target structure, but the left half is estimated as being shallower and the right half as being deeper than the target.

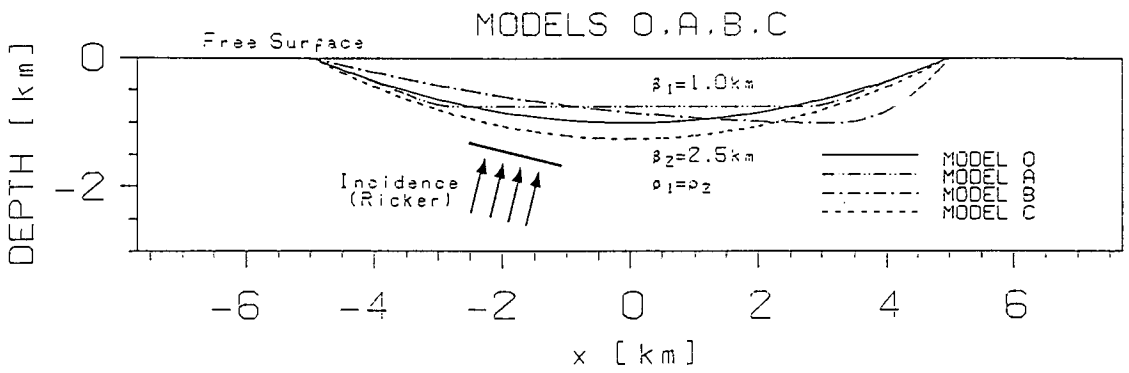
MODELS O,A,B,C
Free Surface
0
-2
DEPTH [km]
β1=1.0km
β2=2.5km
ρ1=ρ2
Incidence
(Ricker)
MODEL O
MODEL A
MODEL B
MODEL C
-6
-4
-2
0
2
4
6
x [km]

Fig. 1

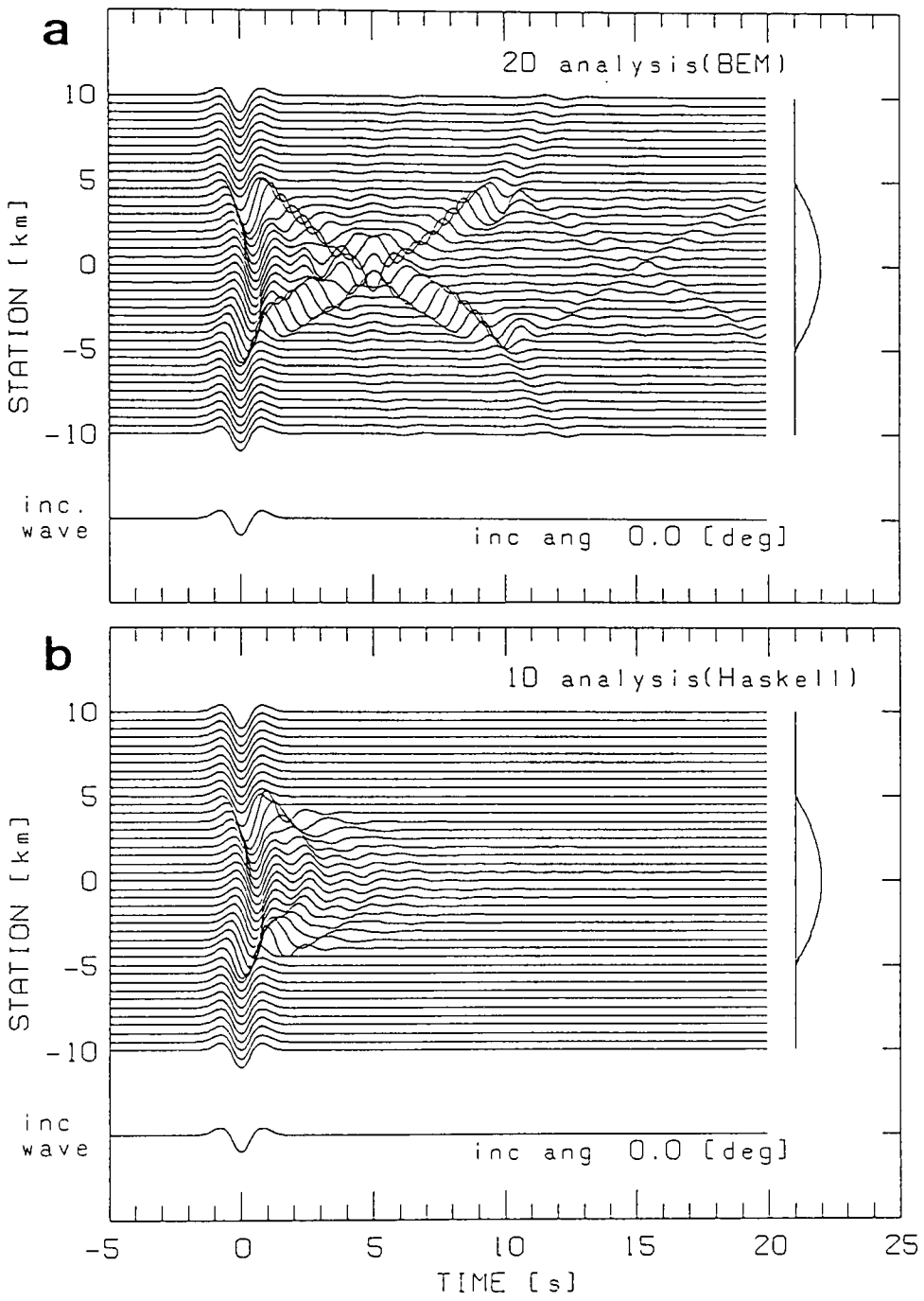
Seismograms for Model 0
a
2D analysis(BEM)
10
5
0
-5
-10
STATION [km]
inc.
wave
inc ang 0.0 [deg]
b
1D analysis(Haskell)
10
5
0
-5
-10
STATION [km]
inc
wave
inc ang 0.0 [deg]
-5
0
5
10
15
20
25
TIME [s]

Fig. 2

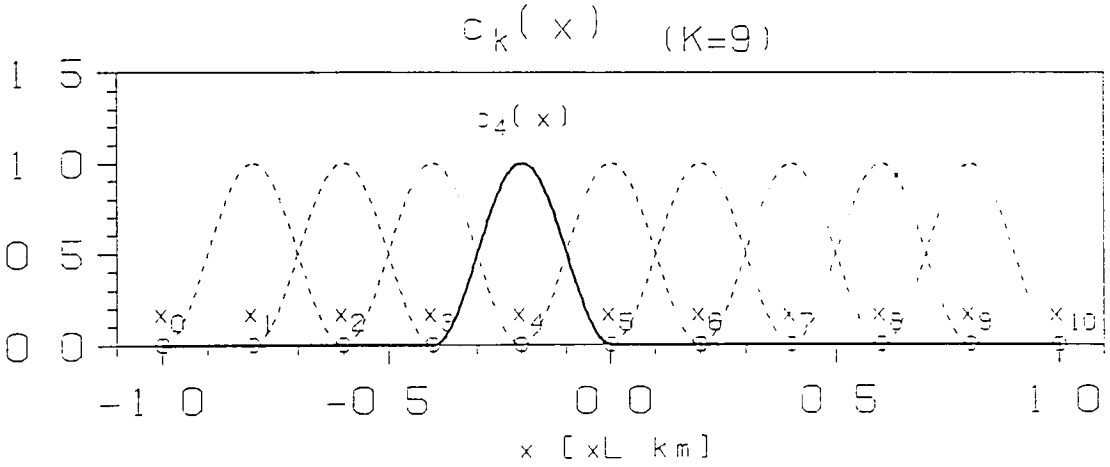
$c_k(x)$ (K=9)
$c_4(x)$
1 5
1 0
0 5
0 0
x_0
x_1
x_2
x_3
x_4
x_5
x_6
x_7
x_8
x_9
x_{10}
-1 0
-0 5
0 0
0 5
1 0
x [xL km]

Fig. 3

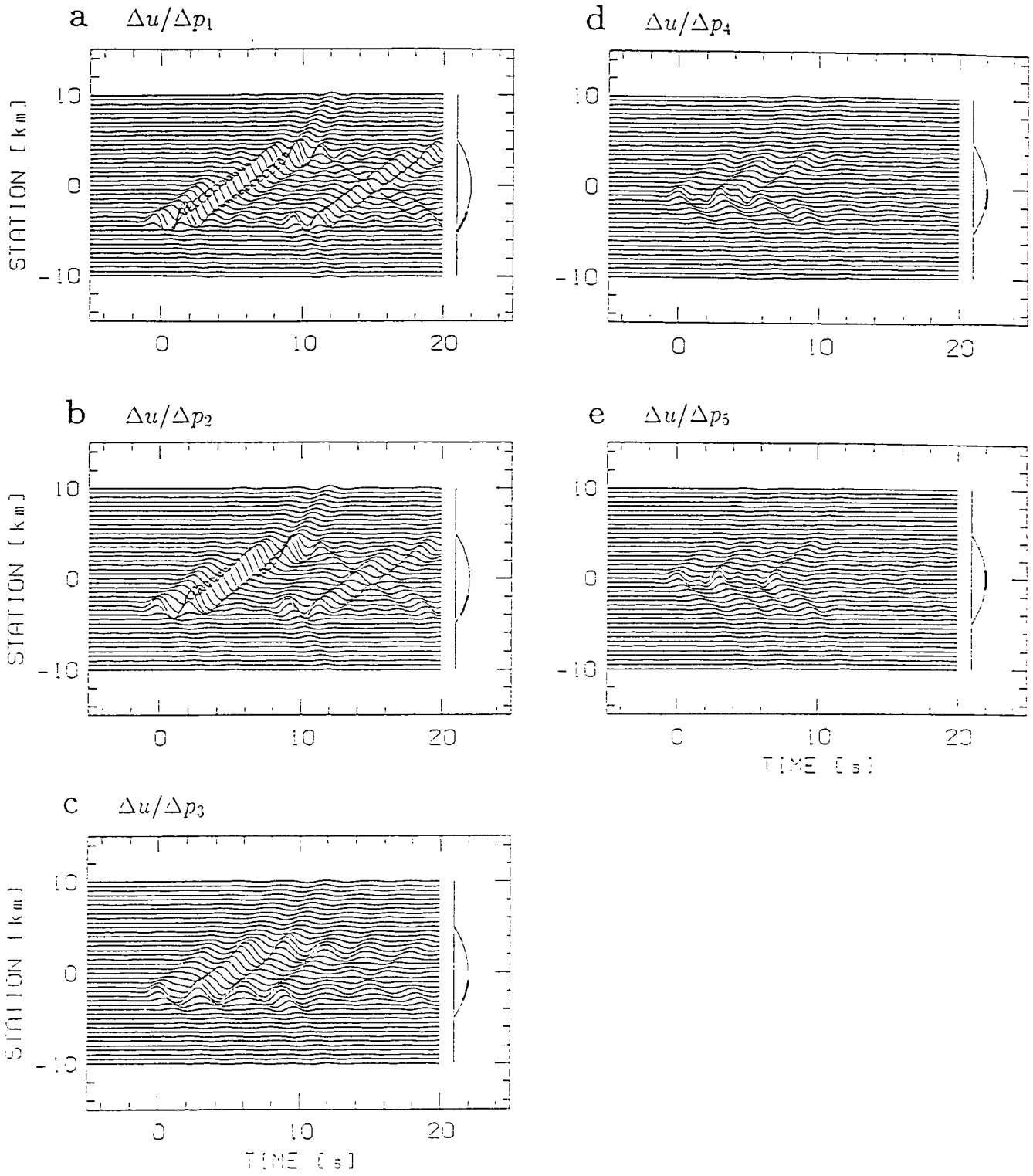
a $\Delta u/\Delta p_1$
b $\Delta u/\Delta p_2$
c $\Delta u/\Delta p_3$
d $\Delta u/\Delta p_4$
e $\Delta u/\Delta p_5$
STATION [km]
10
0
-10
0
10
20
TIME [s]

Fig. 4

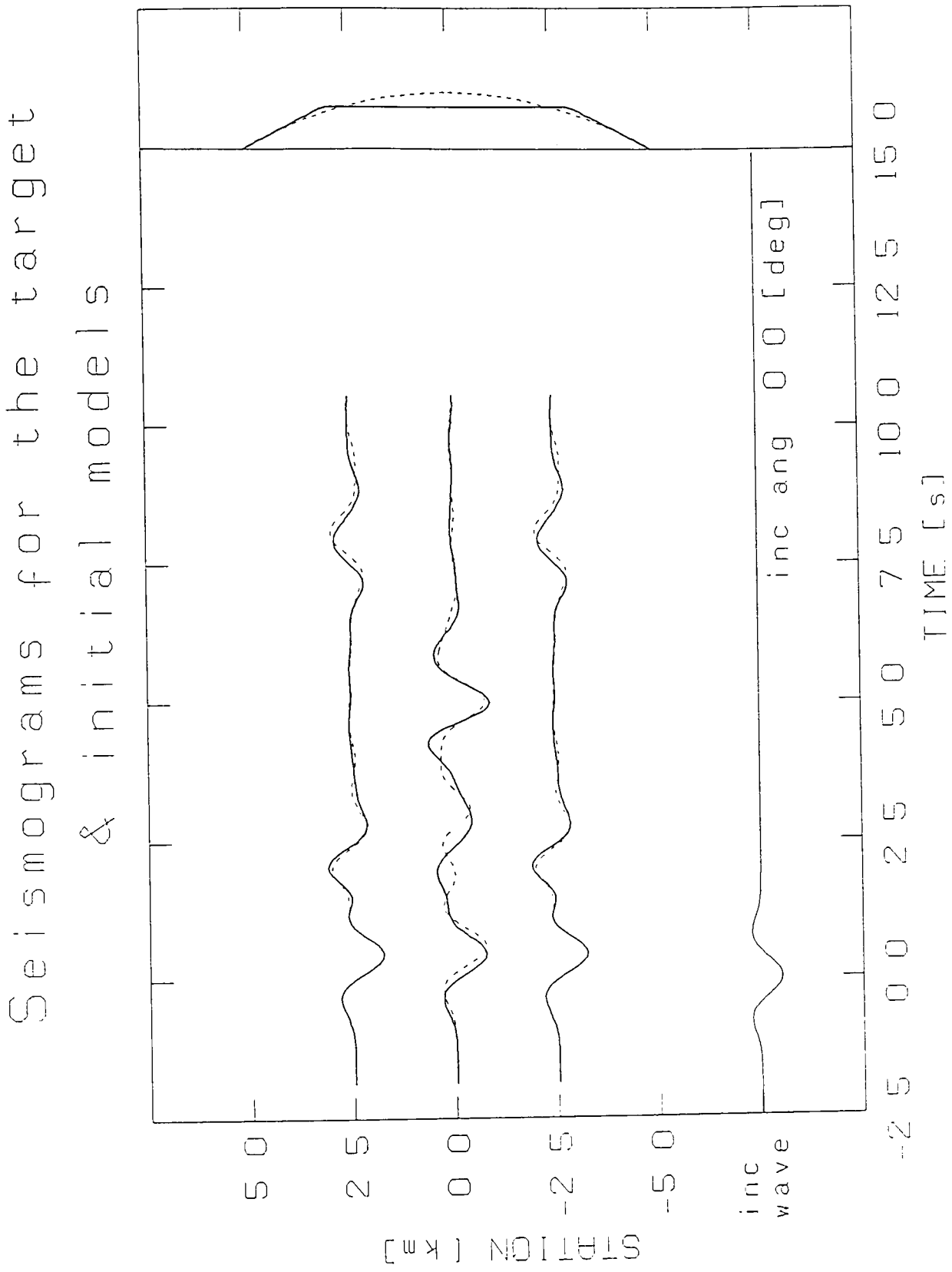
Seismograms for the target
& initial models
inc ang 0.0 [deg]
inc wave
STATION [km]
5.0
2.5
0.0
-2.5
-5.0
-25.00
25.50
75.100
125.150
TIME [s]

Fig. 5

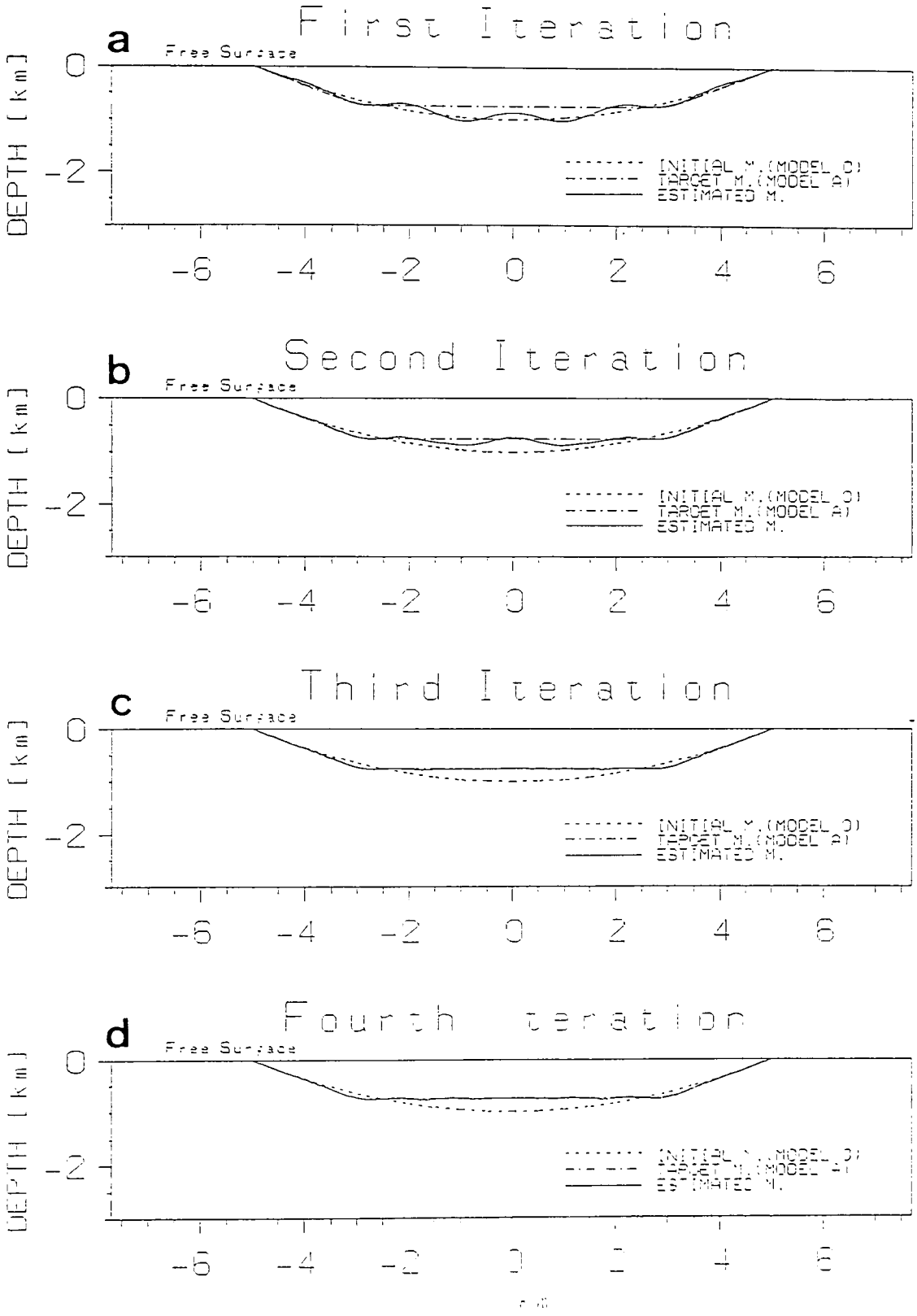
First Iteration
a
Free Surface
DEPTH [km]
0
-2
-6
-4
-2
0
2
4
6
INITIAL M.(MODEL 0)
TARGET M.(MODEL A)
ESTIMATED M.
Second Iteration
b
Free Surface
DEPTH [km]
Third Iteration
c
Free Surface
DEPTH [km]
Fourth Iteration
d
Free Surface
DEPTH [km]

Fig. 6

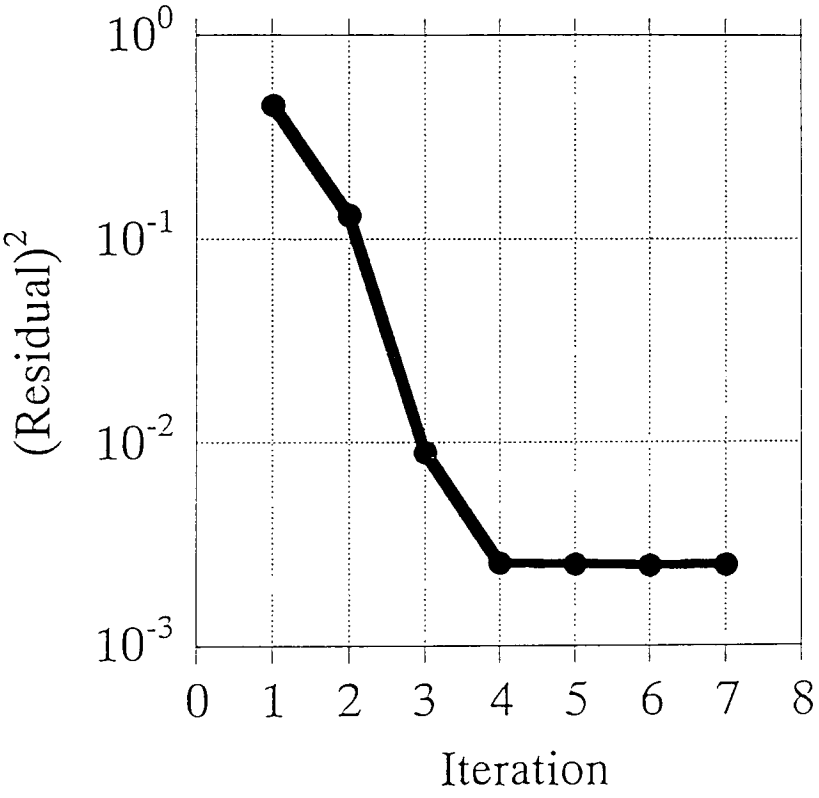

Fig. 7

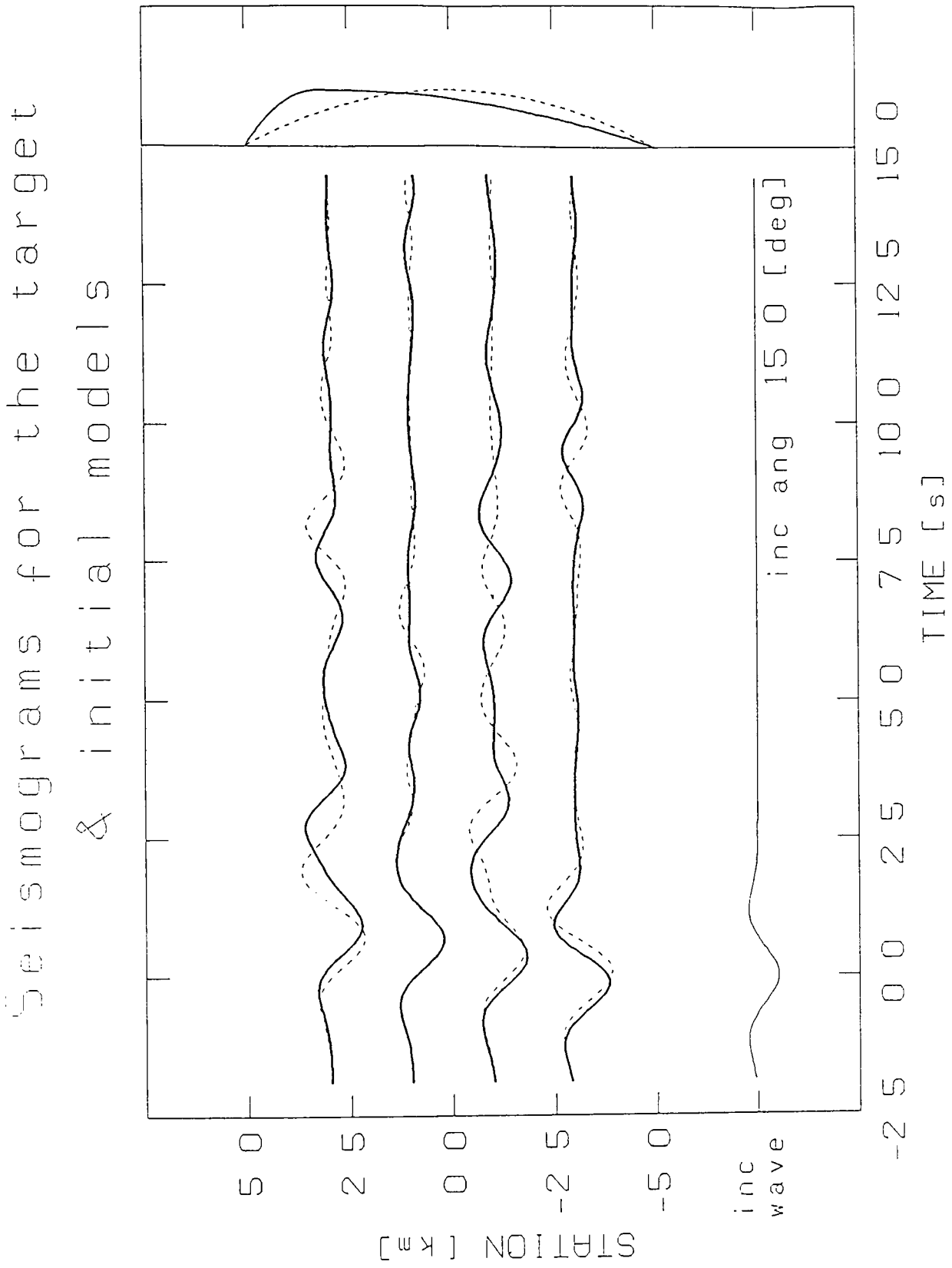
Seismograms for the target
& initial models
STATION [km]
50
25
00
-25
-50
inc wave
inc ang 150 [deg]
-25 00 25 50 75 100 125 150
TIME [s]

Fig. 8

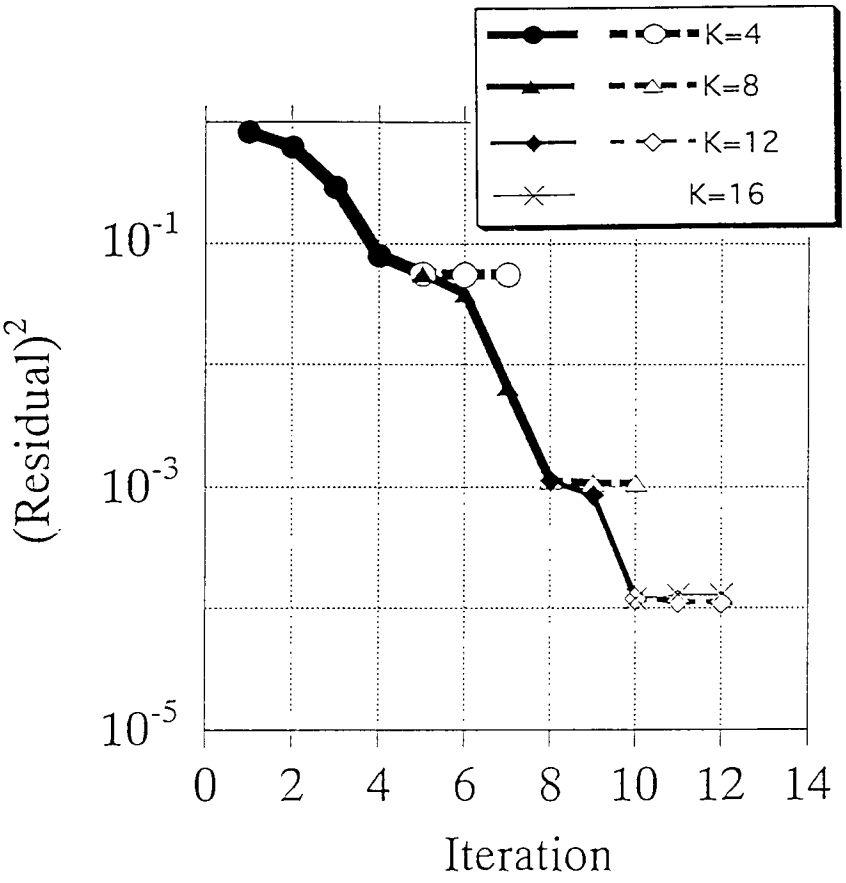

Fig. 9

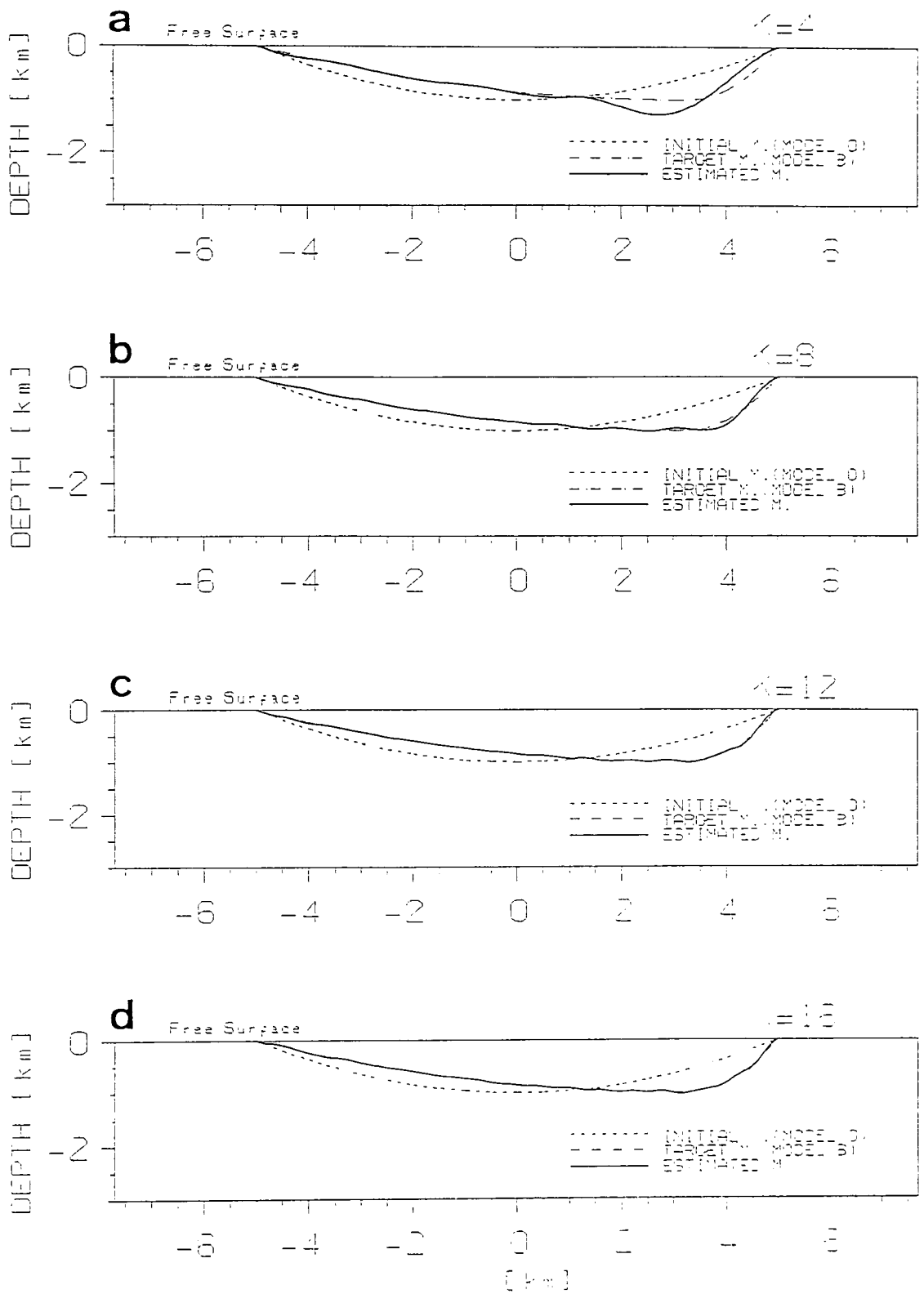
a
Free Surface
DEPTH [km]
0
-2
-6
-4
-2
0
2
4
b
Free Surface
DEPTH [km]
c
Free Surface
DEPTH [km]
d
Free Surface
DEPTH [km]
[km]

Fig. 10

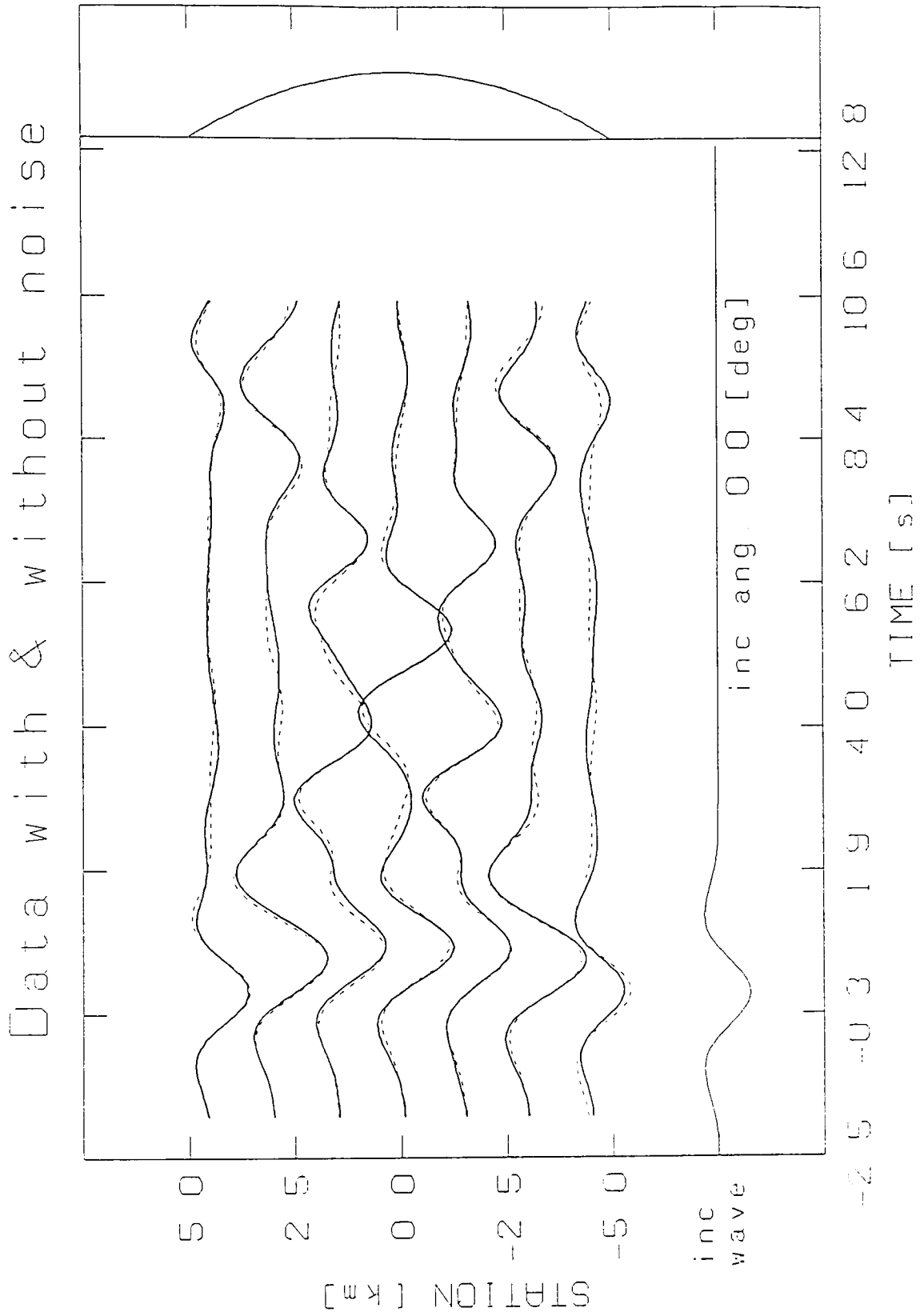
Data with & without noise
STATION [km]
50
25
0
-25
-50
inc wave
inc ang 0.0 [deg]
-2.5
-0.3
1.9
4.0
6.2
8.4
10.6
12.8
TIME [s]

Fig. 11

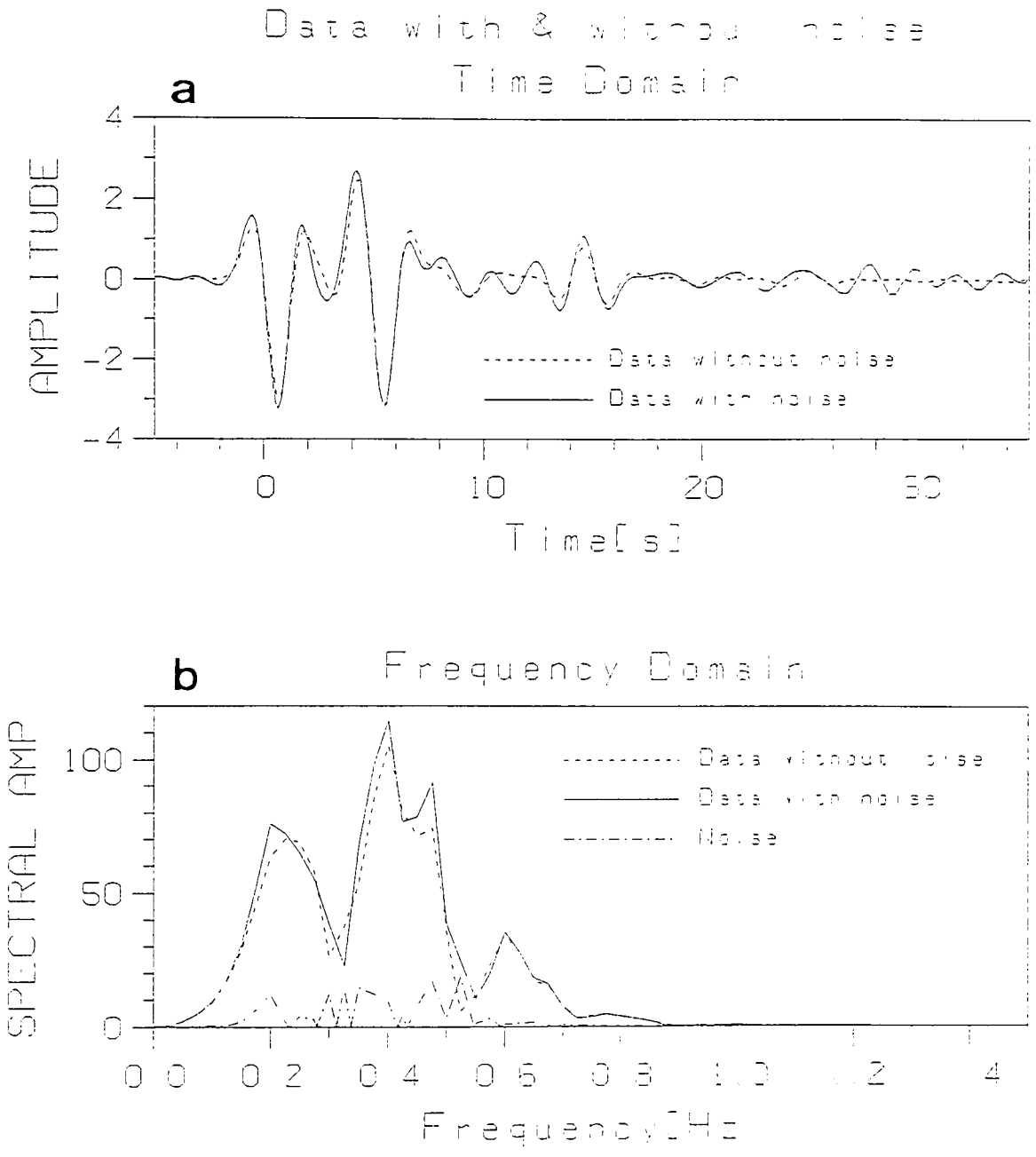
Data with & without noise
Time Domain
a
AMPLITUDE
4
2
0
-2
-4
0
10
20
30
Time[s]
Data without noise
Data with noise
b
Frequency Domain
SPECTRAL AMP
100
50
0
0.0
0.2
0.4
0.6
0.8
1.0
2
4
Frequency[Hz]
Data without noise
Data with noise
Noise

Fig. 12

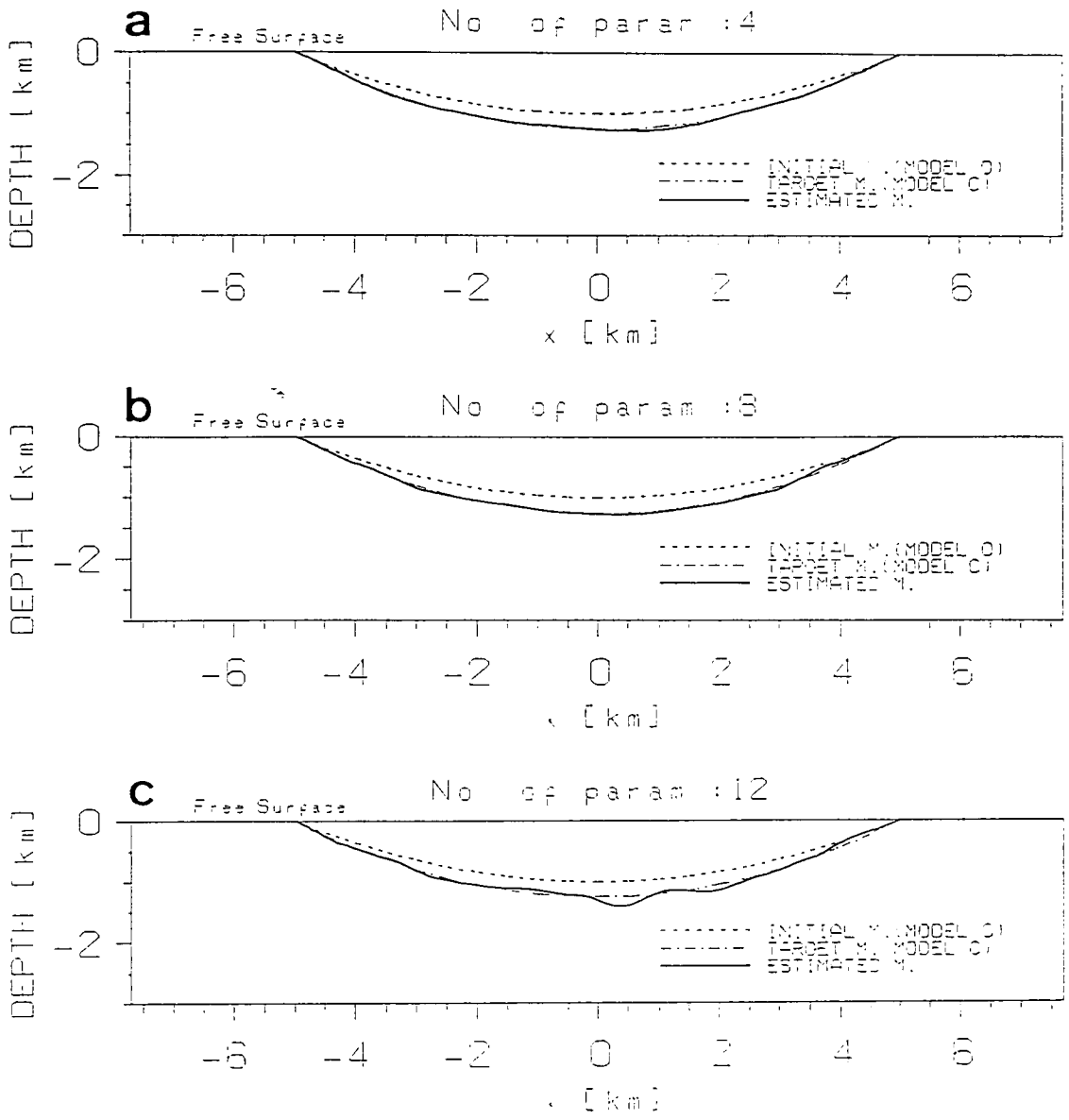
a
Free Surface
No of parar :4
DEPTH [km]
0
-2
-6
-4
-2
0
2
4
6
x [km]
b
Free Surface
No of param :8
DEPTH [km]
0
-2
-6
-4
-2
0
2
4
6
[km]
c
Free Surface
No of param :12
DEPTH [km]
0
-2
-6
-4
-2
0
2
4
6
[km]

Fig. 13

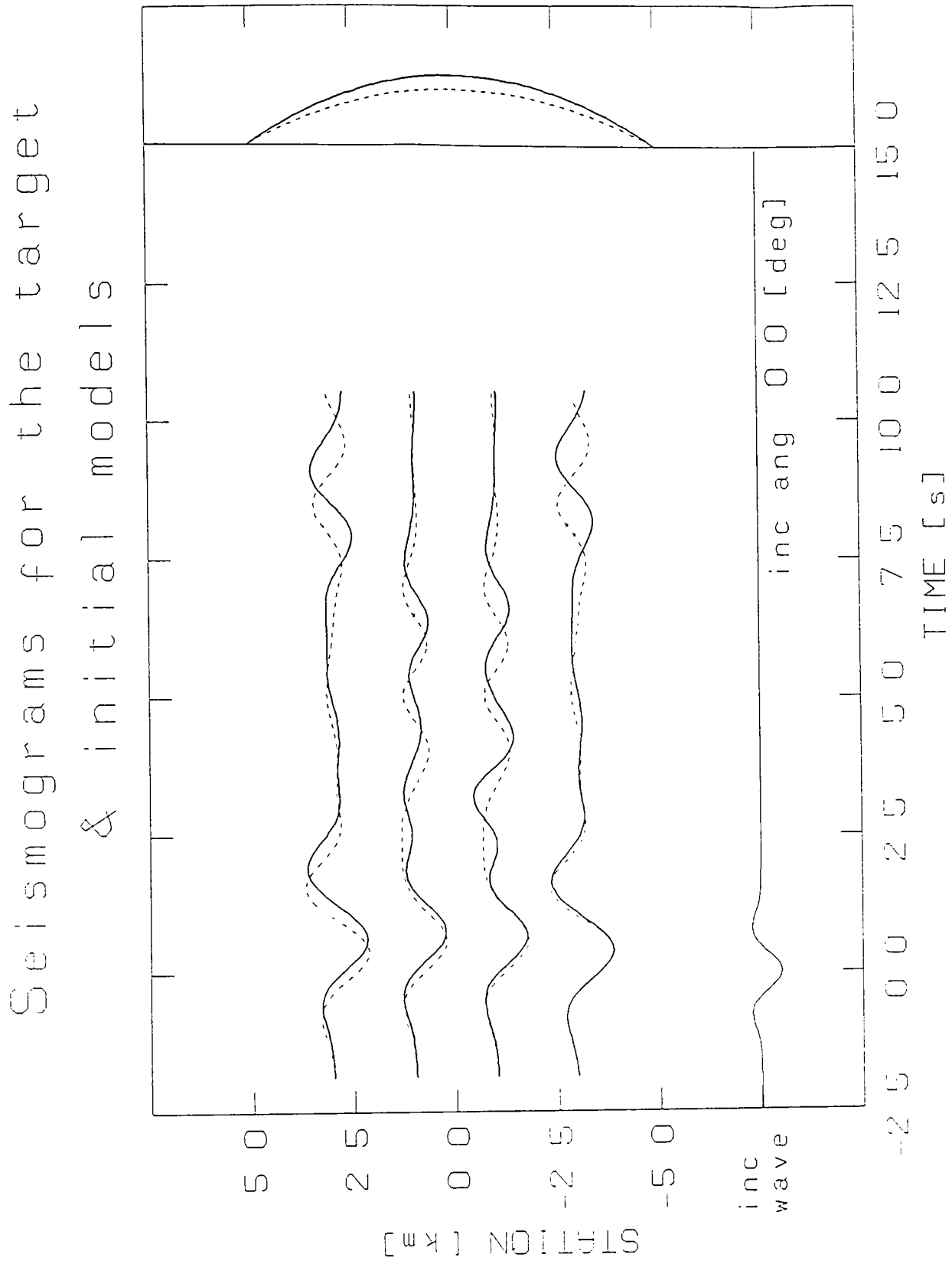
Seismograms for the target
& initial models
inc ang 0 0 [deg]
TIME [s]
-2 5 0 0 2 5 5 0 7 5 10 0 12 5 15 0
STATION [km]
5 0
2 5
0
-2 5
-5 0
inc
wave

Fig. 14

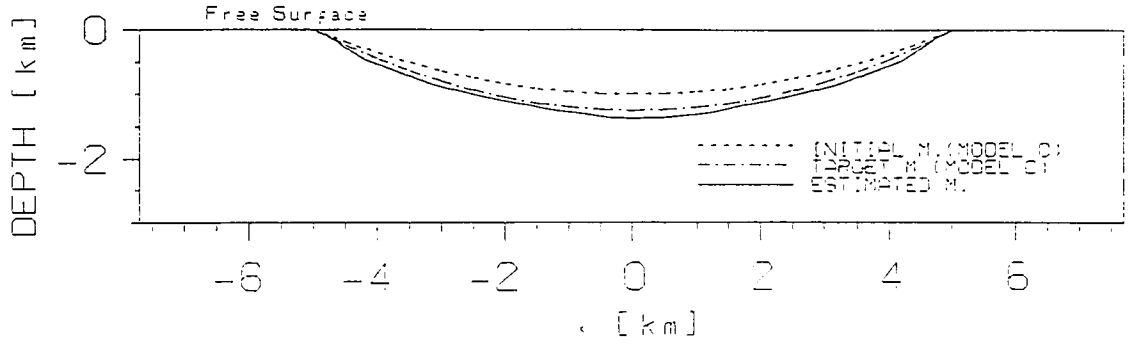
Free Surface
DEPTH [km]
0
-2
-6
-4
-2
0
2
4
6
[km]
INITIAL M.(MODEL_0)
TARGET M.(MODEL_1)
ESTIMATED M.

Fig. 15

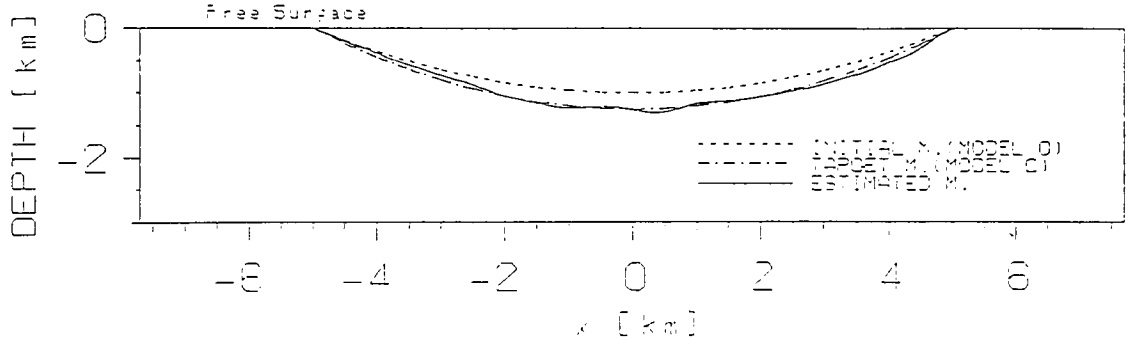
Free Surface
DEPTH [km]
0
-2
-6
-4
-2
0
2
4
6
x [km]
INITIAL M. (MODEL_0)
TARGET M. (MODEL_0)
ESTIMATED M.

Fig. 16

主論文 2

Part II

Boundary Shape Waveform Inversion for Two-Dimensional Basin Structure Using Three-Component Array Data with Obliquely Azimuthal Plane Incident Wave

ABSTRACT

We extended a new waveform inversion scheme for estimating underground structure with an irregular-shaped basement as a target to a case where plane waves impinge on the structure from an azimuthal direction. We proved the validity of this scheme by numerical experiments. We had already achieved the formulation and numerical experiments for the cases where an SH wave impinges on a 2-D basin structure, and had shown that we can estimate the entire basin structure with seismic waveforms from only a few surface stations by using whole waveforms which include the surface waves. However, when the epicenter is located in an obliquely azimuthal direction to the structure, even the cases of 2-D structure cannot be treated as a simple 2-D (SH or P-SV) problem because of the azimuthally impinging wave. Therefore, by dealing with 3-D wavefields in the present study, we extended the inversion scheme in order to be able to apply it to incident waves which impinge from any azimuthal direction. The differential seismograms, which are the sensitivity of change in the waveform, show different patterns in

three components, and we demonstrated that inversion with three components, compared with the inversion with only one of them, gives a linearized equation system with a smaller condition number and a more stable computation. Furthermore, we detected certain parts which are estimated with much less difficulty than others which are not, depending on the direction from which the incident wave impinged. In the latter case, we could estimate the entire structure by simultaneously employing several data from incident waves arriving from different directions. We thus demonstrated by the use of numerical experiments that the extension of our inversion method to cases where the incident wave impinges on the structure from an azimuthal direction enables us to estimate with increased accuracy an underground structure under more general conditions.

INTRODUCTION

The detailed knowledge of an underground structure is very important, since the effects of the basin structure on the waveforms observed on the surface during an earthquake are enormous (e.g., Beck and Hall, 1986, Kawase and Aki, 1989, Yamanaka et al., 1989). In order to estimate the underground structure, many methods such as the refraction and reflection methods have been proposed. However, there are certain difficulties concerning these methods. On one hand, with the refraction method, basically one can estimate only the structure which is located directly underneath the observation station since the data used is only the arrival time. The method does not allow us to perform a high resolution analysis with data from a small number of observation stations. As to the reflection method, on the other hand, the acquisition of records is extremely bothersome, and requires the artificial sources.

The inversion method, which uses the observed data to find their causes, is attracting the attention in many fields because of their objectivity. For instance, tomography techniques are widely

used to estimate underground structure in the field of seismology. However, a high resolution analysis with the existing tomography technique requires numerous (several thousands or ten thousands) parameters. Thus, we proposed a new method to perform an inverse analysis of basin structure, which treats this problem as a domain/boundary inverse problem and requires much smaller number of parameters (Aoi et al. 1995). The domain/boundary inversion (Kubo, 1992) is a method to formulate the inverse problem by paying particular attention to the boundary shapes of several regions regarded as homogeneous. The method has already been used for ten years in mechanical engineering (Barone and Caulk, 1982). For example, non-destructive inspection has been carried out to determine the shapes and locations of cavities or cracks in metal by using the data from the measurements such as electric potentials on the surface (e.g., Nishimura and Kobayashi, 1991, Tanaka and Yamagiwa, 1988, Kubo et al., 1988). However, there are only a few applications of the domain/boundary inversion to seismology (Nowack and Braile, 1993, White, 1989).

Concerning the basin structure treated in the present study,

since the impedance ratio is quite large between a hard basement with a high wave velocity and a soft sedimentary layer with a low wave velocity, we can consider that each of them consists of an approximately homogeneous elastic medium. By choosing a boundary shape with large impedance ratio between the basement and the sedimentary layer as a target parameter, we could perform the inversion with just several dozens of parameters. In this way, we carried out a formulation and numerical experiments for cases where an SH wave impinges on a 2-D basin structure, and showed the validity of this method and its robustness against noise. A significant difference between the inversion of underground structure in seismology and non-destructive inspection in mechanical engineering is that in the former the observation stations as well as sources are spatially maldistributed. In more concrete terms, as to non-destructive inspection, one can determine the locations of observation points or sources in such a way that they encircle the object, while in most seismic observations, the measurements have to be made on the surface. The source locations are limited even for natural earthquakes as well as for artificial sources. Consequently,

it was difficult to obtain sufficient data for carrying out the inversion. In order to overcome those difficulties, we decided to employ the waveform inversion which uses as data the entire waveform instead of limited information such as the arrival times. We came to the conclusion that in cases where a plane SH wave impinges on a 2-D double-layered structure, the use of surface waves generated secondarily by the structure enables us to completely estimate the entire structure with data from only a few observation stations (Aoi et al. 1995).

In the present study, we extended the previous method explained above to cases where the incident waves impinge on the structure from an obliquely azimuthal direction. We consider the incident wave corresponding to the deep earthquake approximately as plane wave. When the epicenter is located out of a plane including the measurement points, the direction from which the incident waves impinge is obliquely azimuthal to the 2-D structure. In these circumstances, even the cases for 2-D structure cannot be treated as simple 2-D (SH or P-SV) problems because of the incident wave from an azimuthal direction. Therefore, we extended the inversion

to the so-called 2.5-D problem, that deals with 3-D wavefields for 2-D structures, so that we would be able to apply it to incident waves which impinge from any azimuthal direction (e.g., Fujiwara 1995, Pedersen et al. 1995, Pei and Papageorgiou 1993). First of all, since three components in the differential seismograms show different patterns, it is preferable to carry out the inversion with three components than doing so with only one of them. This will be shown by the examination of condition number of linearized equation. Secondly, we will demonstrate that certain parts of the structure are easier to estimate than others depending on the arrival direction of the incident wave. We will successfully perform the inversions by simultaneously using the data from several incident waves arriving from different directions. Conclusively, we will describe that the extension of the present method to cases of incident waves impinging on the structure from an obliquely azimuthal direction enables us to perform the inversion with increased accuracy under more general conditions.

CONFIGURATION OF THE MODEL AND THE INCIDENT WAVE

Fig. 1 shows our assumed 2-D basin structure model, which lies along the y-axis and consists of two homogeneous, isotropic, elastic mediums corresponding to a sedimentary layer and a basement. We will consider a case where the plane incident wave impinges on this model from obliquely azimuthal direction. We define that the angle formed by the z-axis and the wavenumber vector of the incident wave is the incident angle θ, and that the angle formed by the negative x-axis and the projection of the wavenumber vector on the xy plane, the azimuthal angle φ.

When $\varphi = 0°$, we can completely separate the SH and P-SV wavefields, which implies that it becomes a pure 2-D problem. However, when $\varphi \neq 0°$, we have to treat this as a 2.5-D problem because of the reciprocal coupling of these wavefields. In this study, we carry out the waveform synthesis by using the boundary integral equation method formulated by Fujiwara (1995). By transforming the wave equation in a space-frequency domain to a wavenumber-frequency domain using a Fourier transformation only in the y direction, we obtain an equation which does not depend on y. This allows us to solve the problem of a 3-D wavefield for

plane incident wave impinging from any azimuthal direction within a reasonable computation time, which is only several times longer than that of a P-SV problem.

FUNCTION SYSTEM AND PARAMETERS TO DESCRIBE THE BOUNDARY SHAPE

In order to formulate the boundary shape to be estimated for the inverse problem, the boundary shape has to be discretized and described by several parameters. We denote this boundary shape $\zeta(x)$ as

$$\zeta(x) - \zeta^0(x) = \sum_{k=0}^{K+1} p_k \times c_k(x) \tag{1}$$

where $\zeta^0(x)$ denotes the boundary shape of the initial model. That is, the difference of depth between the initial and the target models is described by the expansion of the function $c_k(x)$. We introduce the following as the function system $\{c_k(x)|k = 0, 1, \cdots, K, K+1\}$,

$$c_k(x) = \begin{cases} \frac{1}{2}\{1 + \cos\frac{\pi}{\Delta}(x - x_k)\} & \text{if } x_{k-1} \leq x \leq x_{k+1} \\ 0 & \text{otherwise} \end{cases} \tag{2}$$

$$c_0(x) = \begin{cases} \sin\frac{\pi}{2\alpha\Delta}(L + x) & \text{if } -L \leq x \leq -L + \alpha\Delta \\ \frac{1}{2}\{1 + \cos\frac{\pi}{(1-\alpha\Delta)}(L - \alpha\Delta + x)\} & \\ & \text{if } -L + \alpha\Delta \leq x \leq -L + \Delta \\ 0 & \text{otherwise} \end{cases} \tag{3}$$

$$c_{K+1}(x) = c_0(-x) \tag{4}$$

where the width of the basin is $2L$ ($-L \leq x \leq L$), and this is divided into $K+1$ pieces, with $K+2$ node points numbered from 0 to $K+1$. Its x coordinate is denoted as x_k. Fig. 2 shows the spatial distribution of the function system $c_k(x)$ when $K = 8$. This function system is obtained by adding $c_0(x)$ and $c_{K+1}(x)$ to the function system used in Aoi et al. (1995). We added these two terms so that we can express the boundary shape with the minimum number of divisions, since the a edge of basin is often steep. Except for the basin edge, the parameter p_k represents the difference in depth between the initial and the target models at x_k

The function system $c_k(x)$ is employed to give the depth at all points by interpolating these parameters.

FORMULATION OF THE INVERSION

We denote the observation equation as

$$u_i(x_m, t_n; \boldsymbol{p}) = \tilde{u}_{imn} \qquad \text{(for all } i, m, n\text{)}. \tag{5}$$

The model parameter $\boldsymbol{p}$ has to satisfy the equation (5) best in the

sense of least square, where

$$\begin{cases} u_i(x_m, t_n; \boldsymbol{p}) & : \text{synthetic waveform of } i\text{-th component under a model parameter } \boldsymbol{p} \\ \tilde{u}_{imn} & : \text{observed waveform of } i\text{-th component at } x_m \text{ and } t_n \text{ (given)} \\ x_m & : m\text{-th position} \\ t_n & : n\text{-th time sampling} \\ \boldsymbol{p} & : \text{model parameter (vector)} \\ & \quad (p_0, p_1, \cdots, p_K, p_{K+1})^T \end{cases}$$

This observation equation being non-linear, we obtain its solution by a linearized iterative method.

The left side of the observation equation is expanded in the Taylor series about the parameter $\boldsymbol{p}^0$ (the initial model) and is linearized by omitting the higher order terms.

$$u_i(x_m, t_n; \boldsymbol{p}^0) + \sum_{k=1}^{K} \left. \frac{\partial u_i}{\partial p_k} \right|_{\boldsymbol{p}=\boldsymbol{p}_0} \delta p_k \simeq \tilde{u}_{imn}. \tag{6}$$

$\partial u_i / \partial p_k$ represents differential seismograms. Since they cannot be obtained analytically, they are replaced by finite difference approximation.

$$\frac{\partial u_i}{\partial p_k} \simeq \frac{u_i(x_m, t_n; \boldsymbol{p}^0 + \Delta \boldsymbol{p}_k) - u_i(x_m, t_n; \boldsymbol{p}^0)}{\Delta p_k} \tag{7}$$

where Δp_k is an appropriate positive number,

$$\Delta \boldsymbol{p}_k = (0, \cdots, \Delta p_k, \cdots, 0)^T$$

Equation (6) is a simultaneous linear equation with a non-square matrix as its coefficient. We solve this equation by using a singular

value decomposition method (e.g., Nakagawa and Oyanagi, 1982). We constrain the correction value of parameter in such a way that it becomes less than 50% of the depth at the corresponding point of the initial model for each iteration step. We construct the initial model for the next iteration step from this correction value of parameters thus calculated. We use the square sum of the residuals of data in order to judge the degree of convergence. Having performed the iteration by linearized iteration method until this square sum becomes sufficiently small, we consider this converged model as the finally estimated model.

NUMERICAL TESTS OF INVERSION METHOD

Case A:

Fig. 4 shows synthesized waveforms on the surface when a plane SV wave (a Ricker wavelet (Ricker, 1977) with a characteristic period of three seconds) impinges on Model A (Fig. 3 and Tables 1 and 2) with the incident angle $\theta = 30°$ and the azimuthal angle $\varphi = 45°$ In all components, the arrival of the direct waves reflects the thickness of the sedimentary layer at each point, and

these waves are followed by dominant surface waves, secondarily generated by the irregular structure, especially at the edges of the basin. The surface wave in the up-down component, which contains only Reyleigh waves, is not dominant in the shallow part at the left edge, and is generated as the basin gets deeper. With the x component, though the pattern is different, we can observe the similar tendency. In contrast, as for the y component, the surface waves are equally generated from both edges. Each component has thus a complex and different way to generate and propagate waves.

Among these waveforms, we take those at four points on the surface within the basin, shown by •, as our data, and perform the inversion with Model 0 (Fig. 3) as the initial model. The data (solid line) and the waveforms of Model 0 at the corresponding four points (broken line) are overlapping in the Fig. 5. The residuals of each iteration step and the estimated models in each hierarchical step are shown in Fig. 6. First of all, we perform the inversion with $K = 4$. After the fifth iteration where we can see the residuals becoming constant, the inversion is further performed with $K = 8$. In this way, K is increased to $K = 12$, $K = 16$. We conclude that

the model shown in Fig. 6c is the ultimately estimated model from the fact that the residuals do not decrease any more when $K = 12$ is increased to $K = 16$. This final model corresponds perfectly to the target model, Model A, thus showing sufficient accuracy of the estimation of structure.

The arrival direction of incident wave and the estimated model

Case B1:

We will now carry out experiments with a more complex model, Model B (Fig. 3 and Tables 1 and 2) which has a shallow part in the middle. Fig. 7 shows the waveforms that we obtained when a plane SV wave (a Ricker wavelet with characteristic period of three seconds) impinges on this model with the incident angle of $\theta = 30°$ and the azimuthal angle of $\varphi = 45°$ (Case B1a), and Fig. 8 shows a case where the incident angle is $\theta = 30°$ and the azimuthal angle is $\varphi = 135°$ (Case B1b). The waveforms are more complex in Model B than in Model A, because the surface waves are generated secondarily by the irregular structure of the plateau as well as by that at the edges. In Case B1a, the surface waves secondarily generated

from the right end of the plateau and at the right edge of the basin get mixed. Therefore there are many phases at the right side of the plateau. On the contrary, in Case B1b, the surface waves are dominantly generated and many phases are observed at the left side of the plateau. Among these waveforms, we take those at four points on the surface within the basin, shown by •, as our data, and perform the inversion with Model 0 as the initial model. The residuals of each iteration step and the estimated models in each hierarchical step from these inversions in the Case B1a and B1b respectively are shown in Fig. 9 and 10. In both cases, the residuals do not decrease sufficiently (note that the scale of the vertical axis is logarithmic), then the estimation of the structure is not precise. More precisely, only the left side of the structure is more or less correctly estimated in Case B1a, and only the right side is correctly estimated in Case B1b.

The present method enables us to estimate the entire structure with data from a small number of stations because we use not only direct waves but also surface waves. The advantage of the use of the surface wave, which propagates horizontally with information

about the structure underneath, is that it contains more information about underground structure over a wide range compared with the direct wave which has only information concerning the structure just underneath the observation station. In Case B1a, we can correctly estimate the entire shape when we perform the inversion with waveforms from seven surface stations within the basin, indicated by • and o. As we can see in this example, when there are many observation stations, accurate estimation of the entire shape is possible because the large number of direct waves contains sufficient information. However, when there are few observation stations as in Case B1a or B1b, phases overlap, thus making the inverse analysis difficult.

Case B2:

Fig. 11 shows the residuals of each iteration step and the estimated models in each hierarchical step when we carry out the inversion simultaneously using two datasets of Cases B1a and B1b from four surface stations within the basin indicated by •. In this case, the residuals decrease sufficiently and we are able to estimate

the entire structure. As we have seen so far, there are certain parts which are difficult to estimate with the data from only one incident wave in cases of complex structure. In such cases, the simultaneous use of several waveforms from different incident directions enables us to estimate the entire structure with waveforms from a small number of observation stations.

Through the numerical experiments, we are able to find out the locations of observation stations or the arrival direction of incident wave, which are necessary to perform an accurate inverse analysis. In cases where the data are insufficient, we are also able to tell which part of the estimated structure can be trusted. We should then choose this part of the structure as the target of our analysis.

DISCUSSION

Differential seismograms

We show that three components of differential seismograms have different time and space distributions in the simple 2-D case. The top row of Fig. 12 shows the seismograms u_i produced by a Ricker wavelet with a characteristic period of three seconds which

impinges on Model 0 vertically from below. u_x and u_z respectively show waveforms of radial and up-down components when SV wave impinges, and u_y indicates a waveform of transverse component when SH wave impinges. The second row through the sixth row are differential seismograms $\Delta u_i/\Delta p_k$ when K =8, each row corresponding to k =0 through 4. For each $\Delta u_i/\Delta p_k$, the functions $c_k(x)$ corresponding to the parameter p_k with respect to which the seismogram u_i is differentiated, are indicated by broken lines with the basin models, at the right side of the figure.

For all $\Delta u_x/\Delta p_k$ and $\Delta u_y/\Delta p_k$, the direct wave appearing on the waveform just above the parameter to be differentiated as well as the surface waves that propagate from that point are dominant. This characteristic becomes more evident in the differential seismograms corresponding to the parameter near the edge ($k = 1, 2$). However, differential seismograms corresponding to the parameter p_0 do not have large amplitude because the sediment is very shallow close to the edge (around x_0) and the surface waves are not generated secondarily around here. As we have seen, in spite of the common characteristic explained above, the time and space distri-

butions and the amplitude are very different in each component.

Condition number of linearized equation

Since differential seismograms show different patterns for three components, we can imagine that the inversion with three components is more advantageous than the inversion with only one of them. We demonstrate this by examining the condition number of a linearized equation (6).

The condition number κ, which is a quantity related to the propagation law of errors in the equation (e.g., Nakagawa and Oyanagi, 1982), is defined as

$$\kappa = \frac{\mu_1}{\mu_m} \tag{8}$$

μ_1 and μ_m respectively denote the maximum and minimum singular values of the coefficient matrix of the linearized equation. The relative error of the solution is known to be smaller than that of the data multiplied by κ. Because of the noise in data or errors generated by linearized approximation in non-linear problems, it is important to have a small condition number in order to perform a stable inversion.

Here we compare the inversion using three components with that using only one component in a simple 2-D problem where the azimuthal and incident angles are both 0° (vertical incident). We perform the inversion with Model C (Fig. 3 and Tables 1 and 2) as the target model and Model 0 as the initial model. The residuals and the estimated models in each iteration step of the inversion with only one component (SH component) are shown in Fig. 13, and those with both P-SV and SH components, in Fig. 14. Comparing these results, we can see that the condition number is smaller in the latter. We also know that although the final estimation is correct in both cases, it is more unstable in processing the inversion in the case with only one component. Therefore, we conclude that the use of plural components allows us to estimate the basin structure with increased accuracy.

CONCLUSIONS

We extended our new waveform inversion method with boundary shape as its target to cases where the plane wave impinges on the 2-D structure from an obliquely azimuthal direction, and car-

ried out numerical experiments.

Even if the structure is 2-D, this cannot be treated as a simple 2-D problem when the plane wave impinges from an azimuthal direction. Therefore, we treated it as a so-called 2.5-D problem of boundary integral equation method so that we can perform the inversion for plane waves impinging from any obliquely azimuthal direction. Such an expansion enabled us to:

- perform the inversion also in cases where the epicenter has any azimuthal angles to the structure;

- perform a more stable inversion compared to an inversion with only the SH component since we can use waveforms of three components as data.

The latter was demonstrated through the fact that the three components in the differential seismograms, which are the kernels of the inversion, have different patterns; that the condition number of the linearized equation is smaller; that the numerical experiments provide a stable process.

Using the numerical experiments, we also showed that cer-

tain parts in the structure are easier to estimate than others and it depends on the arrival direction of the incident wave. We demonstrated that in such a case, we can estimate the entire structure by simultaneously using the data from incident waves from several directions.

The numerical experiments showed us that the extension of the present inversion scheme to cases where plane waves impinge on the structure from an obliquely azimuthal direction leads us to an estimation with increased accuracy under more general conditions of the epicenter locations.

Acknowledgments

We thank Hiroshi Takenaka and Francisco J. Sánchez-Sesma for their most helpful suggestions. Computation time was provided by the Supercomputer Laboratory, Institute for Chemical Research, Kyoto University.

References

Aoi, S., T. Iwata, K. Irikura and F. J. Sánchez-Sesma (1995). Waveform inversion for determining the boundary shape of a basin structure, *Bull. Seism. Soc. Am.* **85**, 1445-1455.

Barone, M. R. and D. A. Caulk (1982). Optimal arrangement of holes in a two-dimensional heat conductor by a special boundary integral method, *Int. J. Num. Meth. Eng.* **18**, 675-685.

Beck, J. L. and J. F Hall (1986). Factors contributing to the catastrophe in Mexico City during the earthquake of September 19 1985, *Geophys. Res. Lett.* **13**, 593-596.

Fujiwara, H. (1995). Three-dimensional wavefield in a two-dimensional basion structure due to point source, submitted to *J. Phys. Earth.*

Kawase, H. and K. Aki (1989). A study on the response of a soft basin for incident S, P, and Rayleigh waves with special reference to the long duration observed in Mexico City, *Bull. Seism. Soc. Am.* **79**, 1361-1382.

Kubo, S. (1992). *Inverse Problems,* Baifukan, Tokyo (in Japanese).

Kubo, S., T. Sakagami, K. Ohji, T. Hashimoto and Y. Matsumuro (1988). Quantitative Measurement of Three-Dimensional Surface Cracks by the Electric Potential CT Method, *J. Mech. Soc. Japan* A-**54**-498, 218-225

(in Japanese with English abstract).

NAKAGAWA, T. and Y. OYANAGI (1982). *Experimental Data Analysis by the Least-Squares Method,* Univ. of Tokyo Press, Tokyo (in Japanese).

NISHIMURA, N. and S. KOBAYASHI (1991). A boundary integral equation method for an inverse problem related to crack detection, *Int. J. Num. Meth. Eng.* **32**, 1371-1387.

NOWACK, R. L. and L. W BRAILE (1993). Refraction and wide-angle reflection tomography: theory and results, *Seismic Tomography: Theory and Practice*, 733-763.

PEDERSEN H. A., M., CAMPILLO and F J. SÁNCHEZ-SESMA (1995). Azimuth dependent wave amplification in alluvial valleys, *Soil Dynamics and Earthquake Engineering* **14**, 289-300.

PEI, D. and A. S. PAPAGEORGIOU (1993). Study of the response of cylindrical alluvial valleys of arbitrary cross-section to obliquely incident seismic waves using the discrete wavenaumber boundary element method, in *Soil Dynamics and Earthquake Engineering VI* , eds. A. S. CAKMAK, and C. A. BREBBIA, Comp. Mech. Publications — Elsevier Appl. Sc., Southampton-London, pp. 149 -161.

RICKER, N. H. (1977). Transient waves in visco-elastic media, Amsterdam.

TANAKA, M. and K. YAMAGIWA (1988). Application of boundary element

method to some inverse problems in elastodynamics, *J. Mech. Soc. Japan* A-**54**-501, 1054-1060 (in Japanese with English abstract).

WHITE, D. J. (1989). Two-dimensional seismic refraction tomography, *Geophys. J.* **97**, 223-245.

YAMANAKA, H., K. SEO and T. SAMANO (1989). Effects of sedimentary layers on surface-wave propagation, *Bull. Seism. Soc. Am.* **79**, 631-644.

Tables

Table 1. Maximum depths and shapes of the structure models.

	Shape	max. Depth
Model 0	parabola	1.00km
Model A	non-symmetrical parabola	1.00km
Model B	plateau	1.50Km
Model C	parabola	1.25km
width of basin	10km	

Table 2. Physical parameters of Model 0, A, B and C.

	First layer	Second layer
P wave velocity α	2.0 km/s	5.0 km/s
S wave velocity β	1.0 km/s	2.5 km/s
density ρ	1.2 g/cm^3	1.8 g/cm^3
Q-value	∞	∞

Figure Captions

FIG. 1. Configuration of the model and the incident wave. Plane wave with the incident angle θ and the azimuthal angle φ impinges on the 2-D basin structure model which lies along y-axis.

FIG. 2. Examples of the space distribution of the weight function system $c_k(x)$ when K=8. Thin and thick lines show the examples of $c_k(x)$ for $k = 0$ and $k = 4$, respectively.

FIG. 3. Basin structures of Models 0, A, B and C. The physical parameters are shown in Tables 1 and 2.

FIG. 4. Seismograms recorded at surface stations located within the basin for Model A. Incident wave is a Ricker wavelet with a characteristic period of three seconds which impinged on the models with the incident angle $\theta = 30°$ and the azimuthal angle $\varphi = 45°$ Only the waveforms from four stations indicated by • are used for the inversion in Case A. The shape of the underground structure is shown on the right of the top seismogram.

FIG. 5. Waveforms from the four surface stations, indicated by • in Fig. E, which are used for the inversion in Case A (solid line), and the synthetic waveforms for the initial model, Model 0, corresponding to the same four stations (broken line). The shape of the underground structure is shown on the right of the top seismogram.

FIG. 6. Change of the square sum of the residuals after each iteration and the estimated model for the inversion in Case A. The residuals are normalized by that of the initial model. The number of parameters is increased by four each time the residuals converge. The initial (Model 0) and target (Model A) models, and estimated models obtained at each step of the hierarchy are shown respectively by (a) through (d).

FIG. 7. Seismograms recorded at surface stations located within the basin for Model B. Incident wave is a Ricker wavelet with a characteristic period of three seconds which impinged on the models with the incident angle $\theta = 30°$ and the azimuthal angle $\varphi = 45°$ Only the waveforms from four stations shown by • are used for the inversion in Case B1a. We also try to perform the inversion with seven stations shown by • and o. The shape of the underground structure is shown on the right of the top seismogram.

FIG. 8. Seismograms recorded at surface stations located within the basin for Model B. Incident wave is a Ricker wavelet with a characteristic period of three seconds which impinged on the models with the incident angle $\theta = 30°$ and the azimuthal angle $\varphi = 135°$ Only the waveforms from four stations shown by • are used for the inversion in Case B1a. The shape of the underground structure is shown on the right of the top seismogram.

FIG. 9. Change of the square sum of the residuals after each iteration and the estimated model for the inversion in Case B1a. The residuals do not decrease sufficiently (note that the scale of the vertical axis is logarithmic),

and only the left side of the structure is more or less correctly estimated.

FIG. 10. Change of the square sum of the residuals after each iteration and the estimated model for the inversion in Case B1b. The residuals do not decrease sufficiently (note that the scale of the vertical axis is logarithmic), and only the right side of the structure is more or less correctly estimated.

FIG. 11. Change of the square sum of the residuals after each iteration and the estimated model for the inversion in Case B2. The simultaneous use of two waveforms (Case B1a and B1b) enables us to estimate the entire structure.

FIG. 12. Seismograms u_i and the corresponding differential seismograms $\Delta u_i/\Delta p_k$. The top row shows the seismograms produced by a Ricker wavelet with a characteristic period of three seconds which impinges on Model 0 vertically from below. The second to the sixth rows show respectively the differential seismograms $\Delta u_i/\Delta p_k$ of Model 0 for $K = 8$ that correspond to k =0 through 4. For each $\Delta u_i/\Delta p_k$, the shape of the functions $c_k(x)$, which is corresponding to the parameter p_k with respect to which the seismogram u_i is differentiated, are indicated by broken lines with the basin models (solid line), at the right side of the figure.

FIG. 13. Change of the square sum of the residuals and condition number after each iteration and the estimated model for the inversion with only one component (transverse compornent).

FIG. 14. Change of the square sum of the residuals and condition number after each iteration and the estimated model for the inversion with three components.

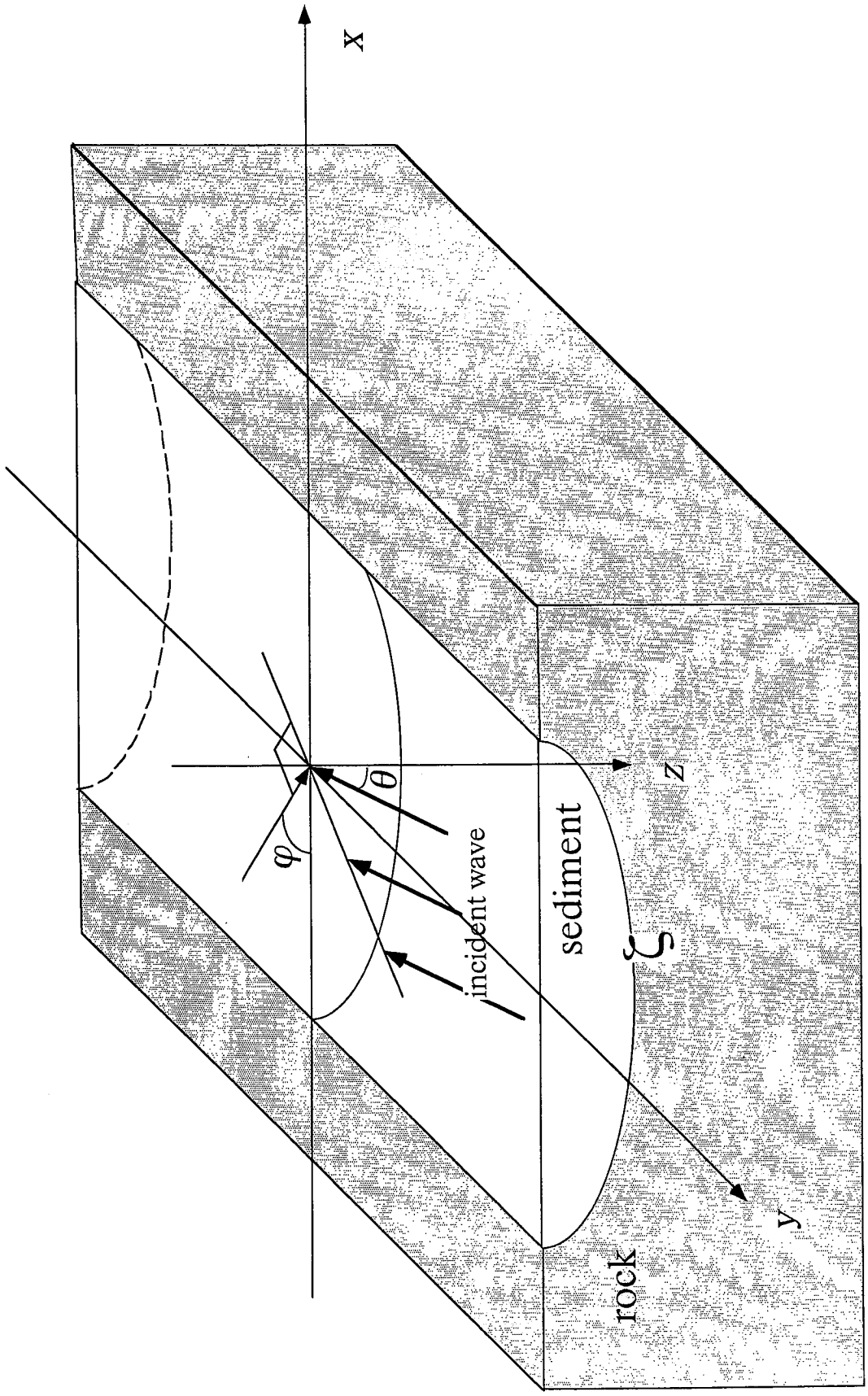

Fig. 1

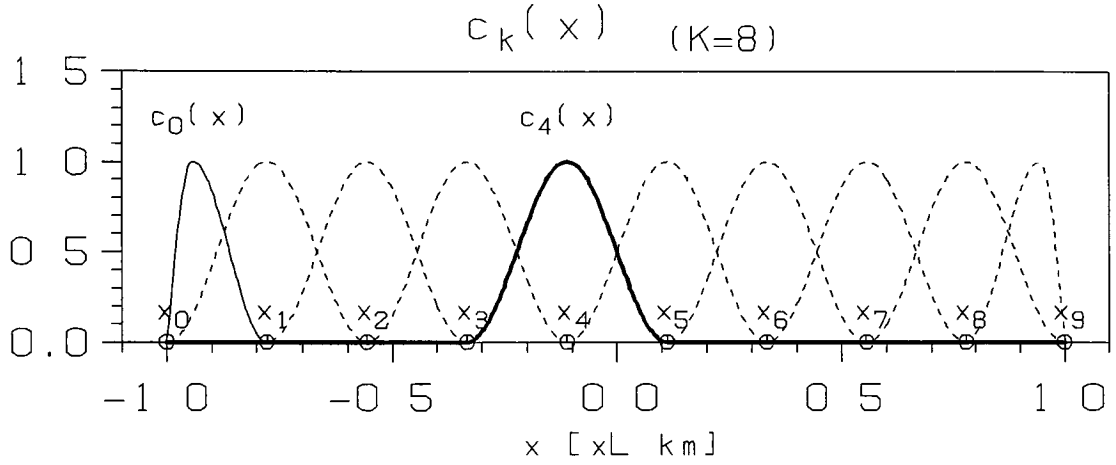
c k (x) (K=8)
1 5
1 0
0 5
0.0
c0(x)
c4(x)
x0
x1
x2
x3
x4
x5
x6
x7
x8
x9
−1 0
−0 5
0 0
0 5
1 0
x [xL km]

Fig. 2

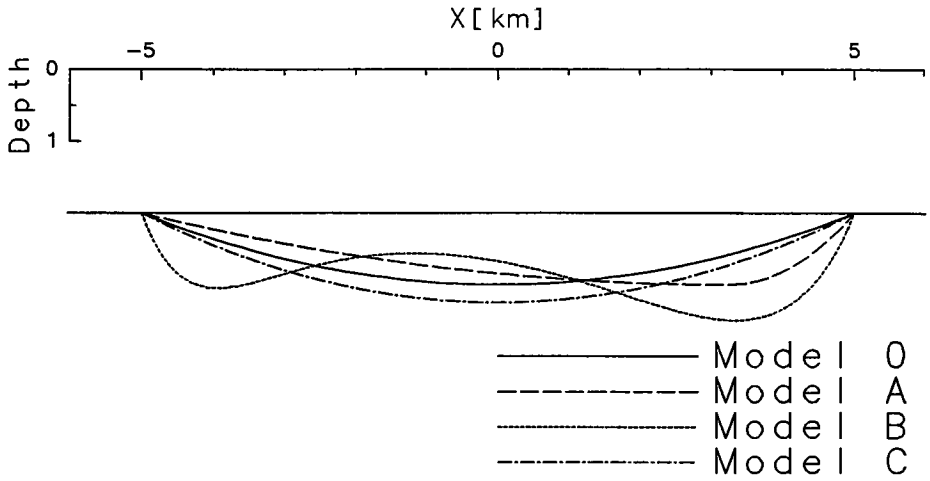

Fig. 3

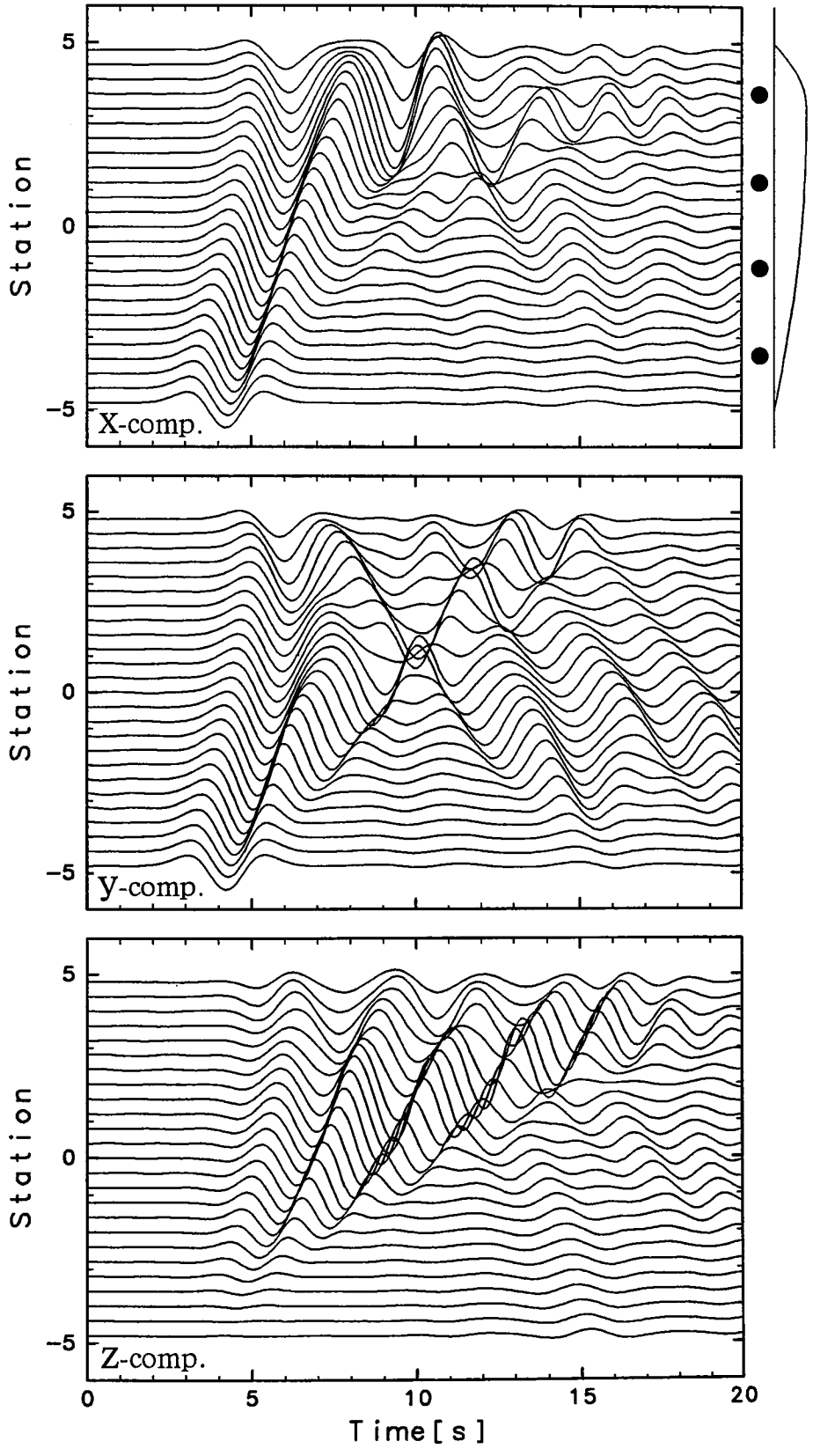

Fig. 4

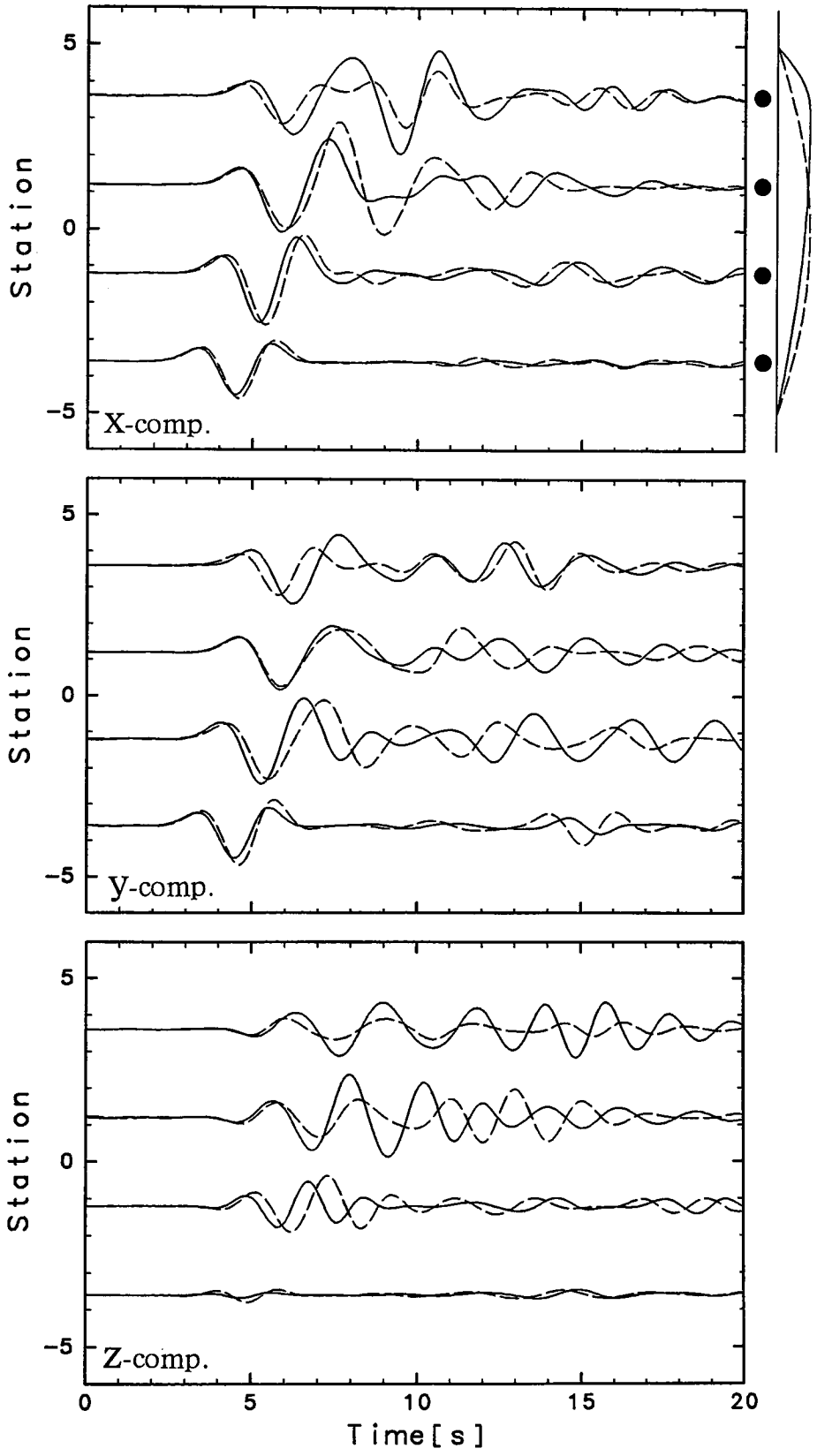
Station
5
0
−5
X-comp.
Station
5
0
−5
y-comp.
Station
5
0
−5
Z-comp.
0
5
10
15
20
Time[s]

Fig. 5

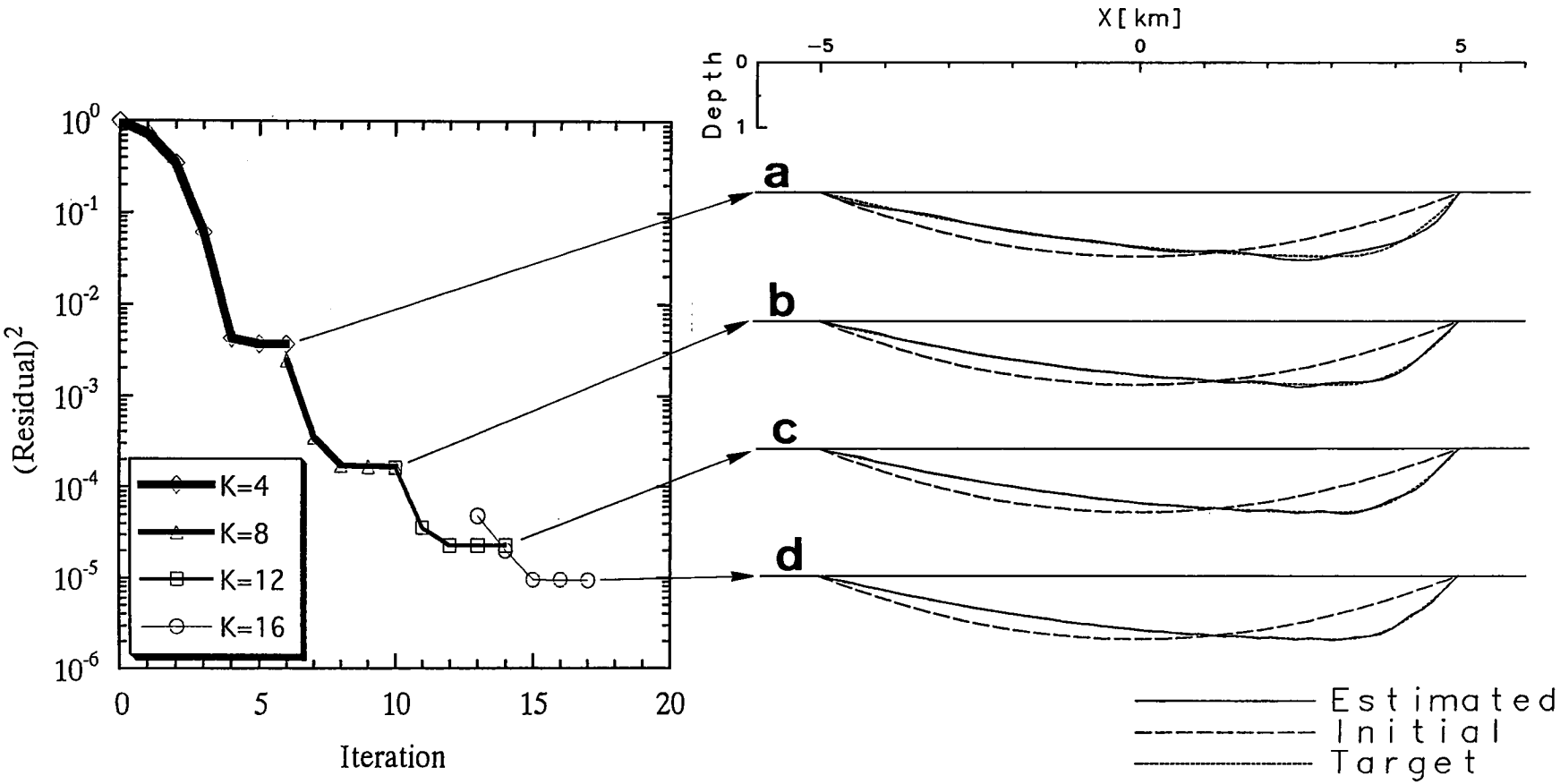
X [km]
−5
0
5
Depth
0
1
a
b
c
d
10^{0}
10^{-1}
10^{-2}
10^{-3}
10^{-4}
10^{-5}
10^{-6}
(Residual)^2
K=4
K=8
K=12
K=16
0
5
10
15
20
Iteration
Estimated
Initial
Target

Fig. 6

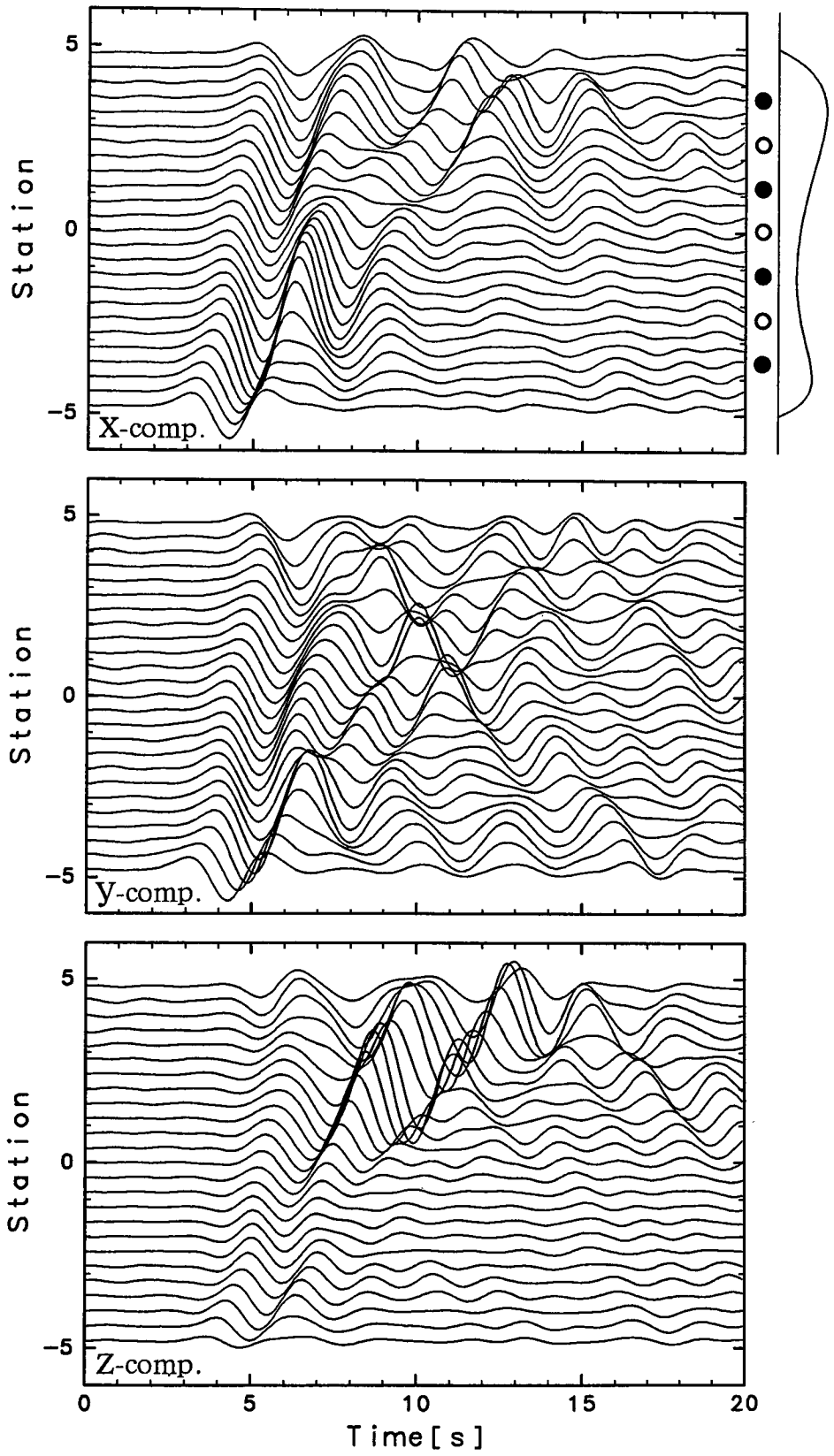
Station
5
0
−5
X-comp.
Station
5
0
−5
y-comp.
Station
5
0
−5
Z-comp.
0
5
10
15
20
Time [s]

Fig. 7

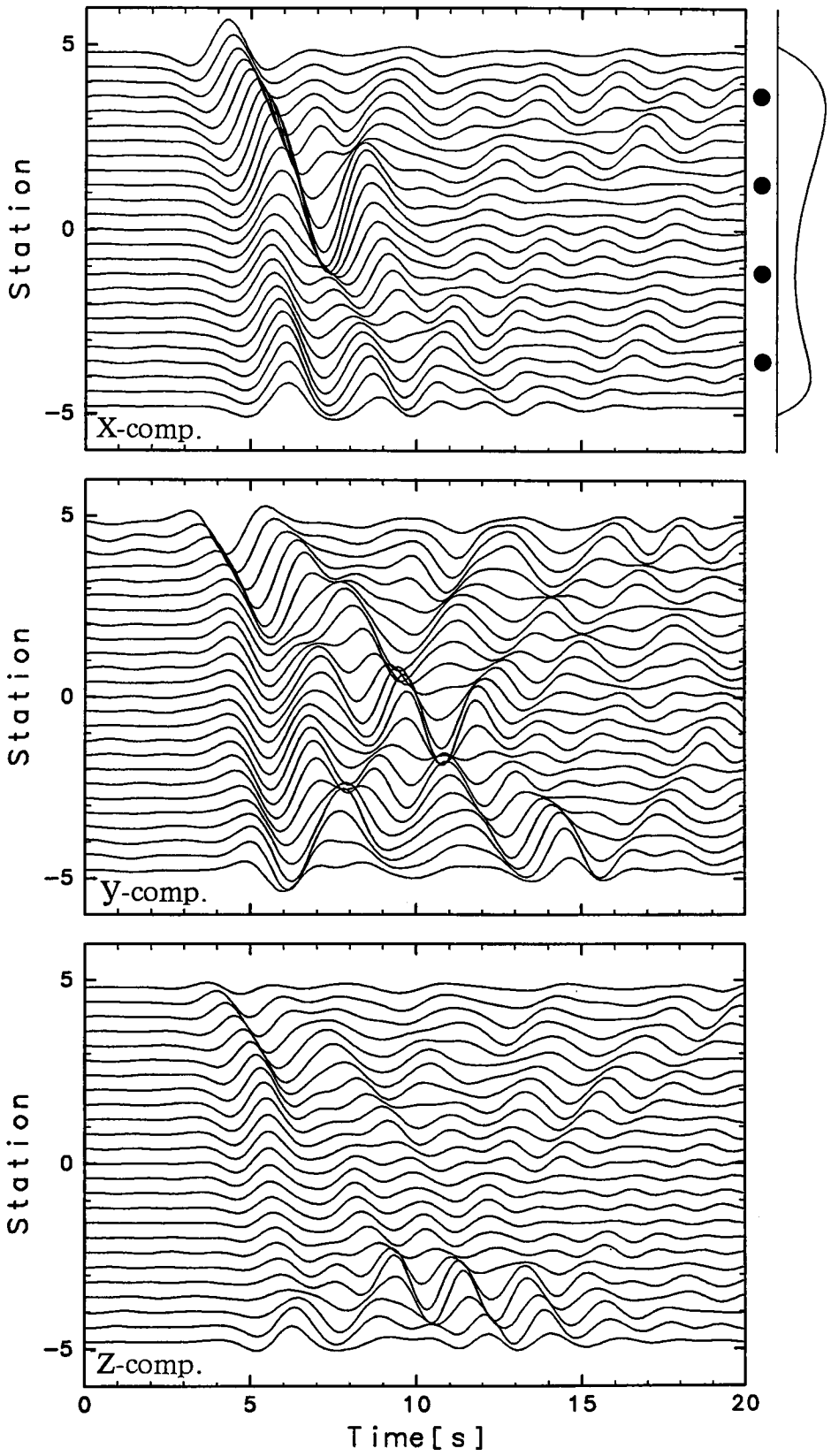
Station
5
0
−5
X-comp.
Station
5
0
−5
y-comp.
Station
5
0
−5
Z-comp.
0
5
10
15
20
Time[s]

Fig. 8

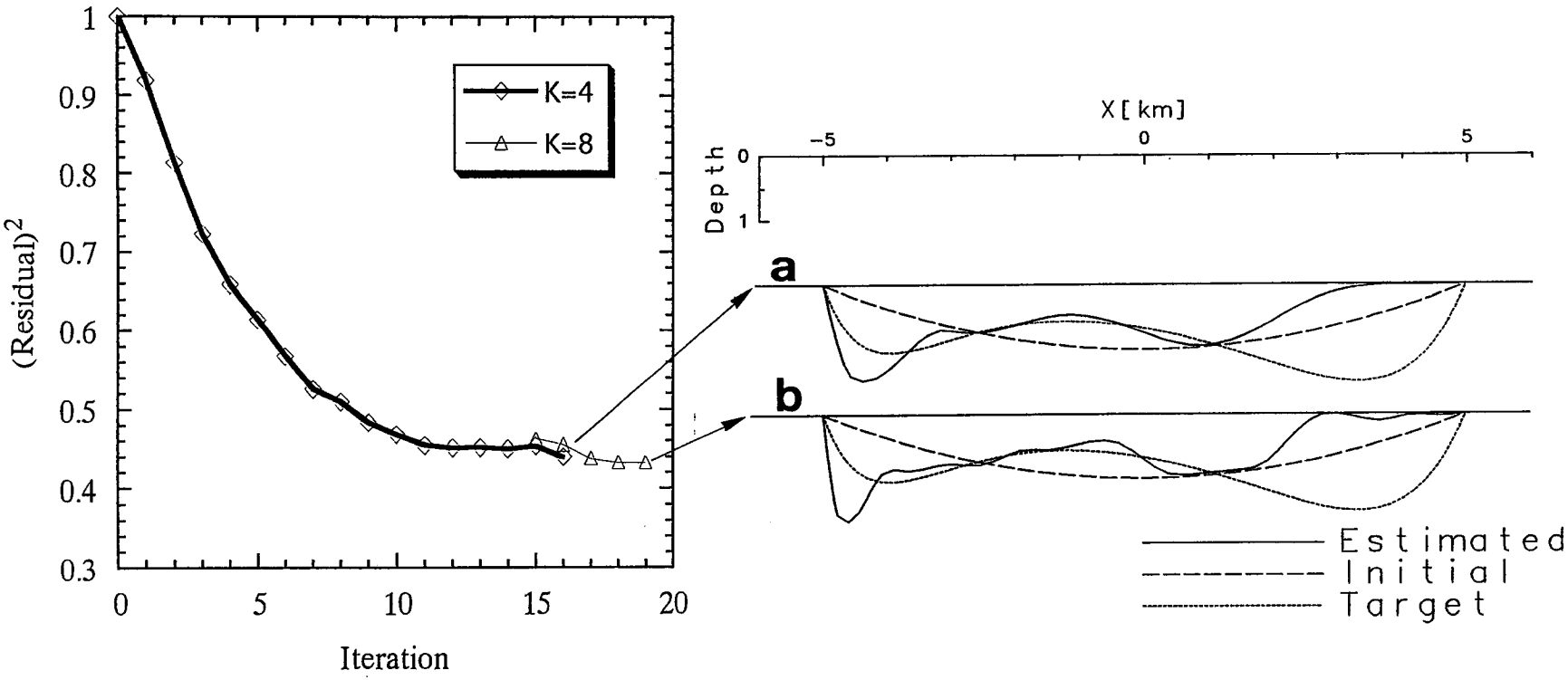
1
0.9
0.8
0.7
0.6
0.5
0.4
0.3
(Residual)^2
0
5
10
15
20
Iteration
K=4
K=8
X [km]
−5
0
5
Depth
0
1
a
b
Estimated
Initial
Target

Fig. 9

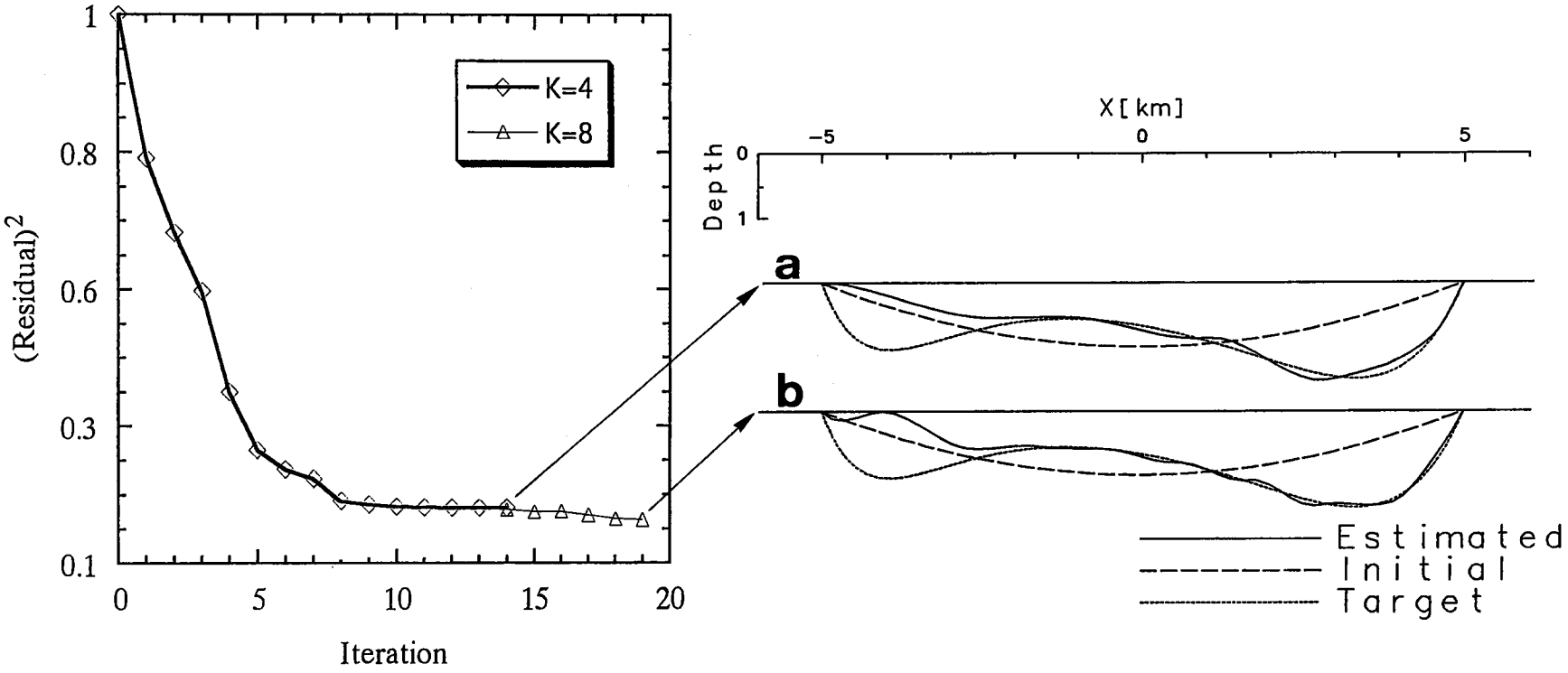
1
0.8
0.6
0.3
0.1
(Residual)^2
0
5
10
15
20
Iteration
K=4
K=8
X [km]
−5
0
5
Depth
0
1
a
b
Estimated
Initial
Target

Fig. 10

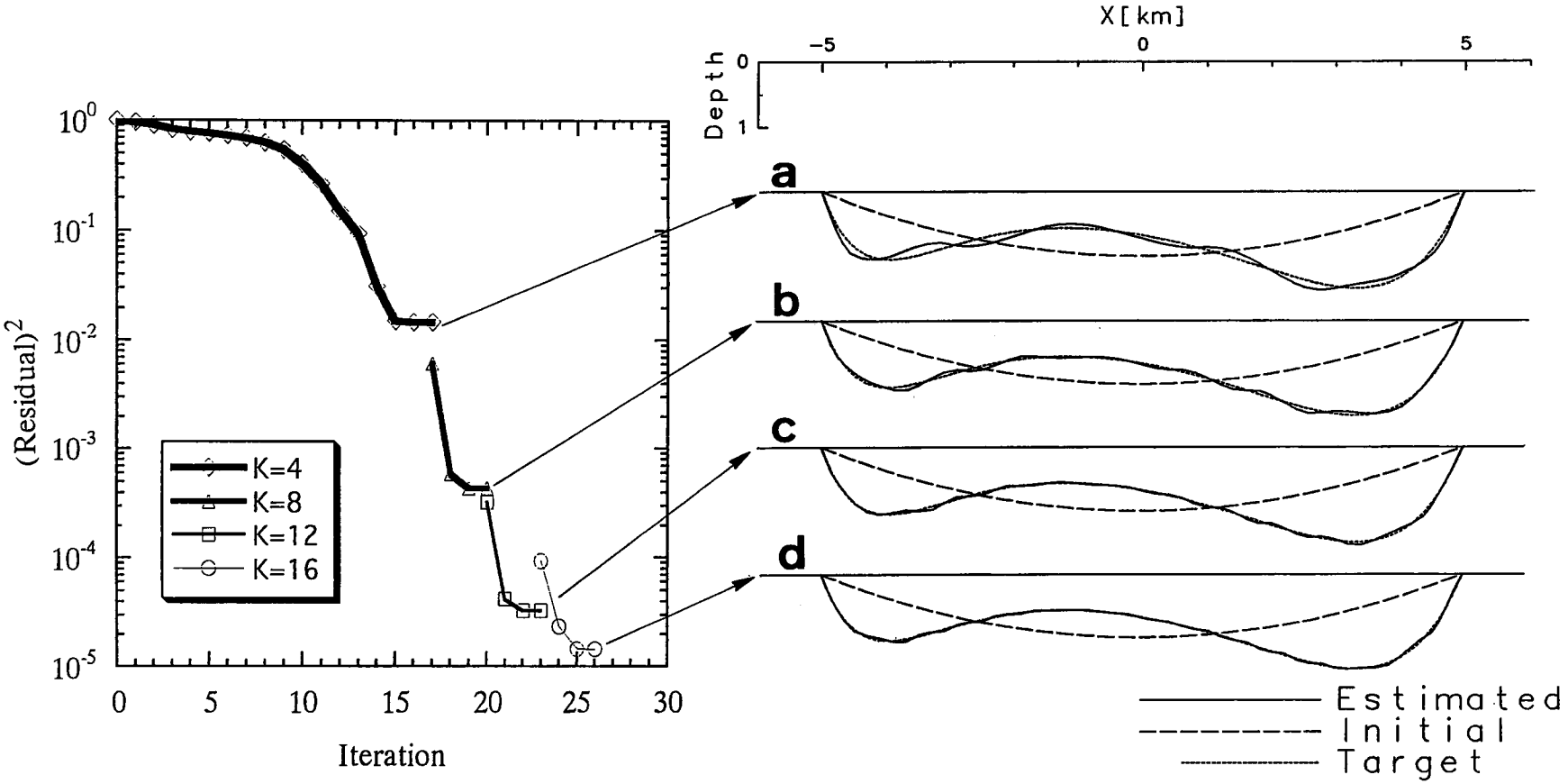
X [km]
−5
0
5
Depth
0
1
a
b
c
d
10^{0}
10^{-1}
10^{-2}
10^{-3}
10^{-4}
10^{-5}
(Residual)^2
K=4
K=8
K=12
K=16
0
5
10
15
20
25
30
Iteration
Estimated
Initial
Target

Fig. 11

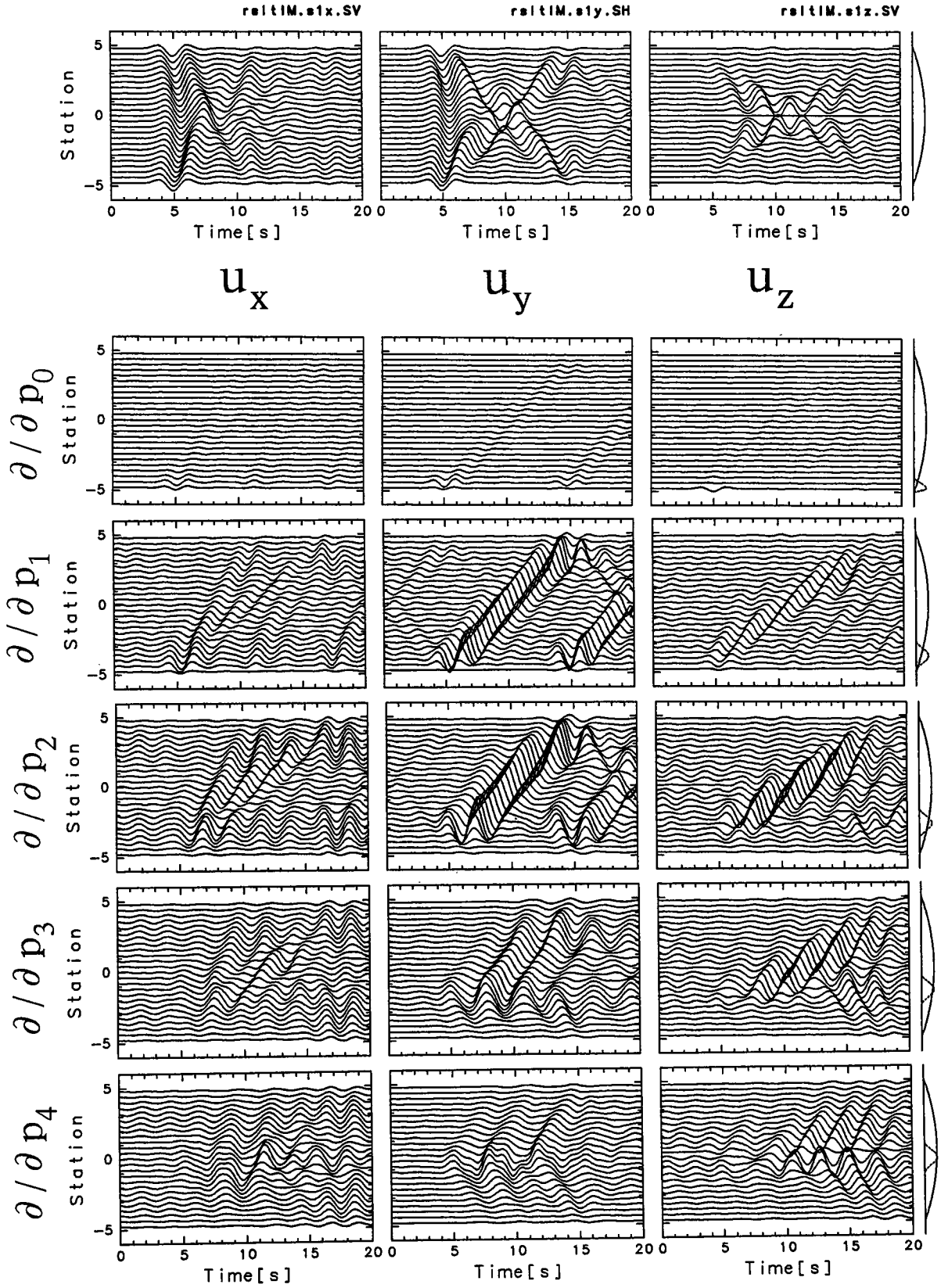
rsltIM.s1x.SV
rsltIM.s1y.SH
rsltIM.s1z.SV
Station
Time[s]
u_x
u_y
u_z
$\partial / \partial p_0$
$\partial / \partial p_1$
$\partial / \partial p_2$
$\partial / \partial p_3$
$\partial / \partial p_4$

Fig. 12

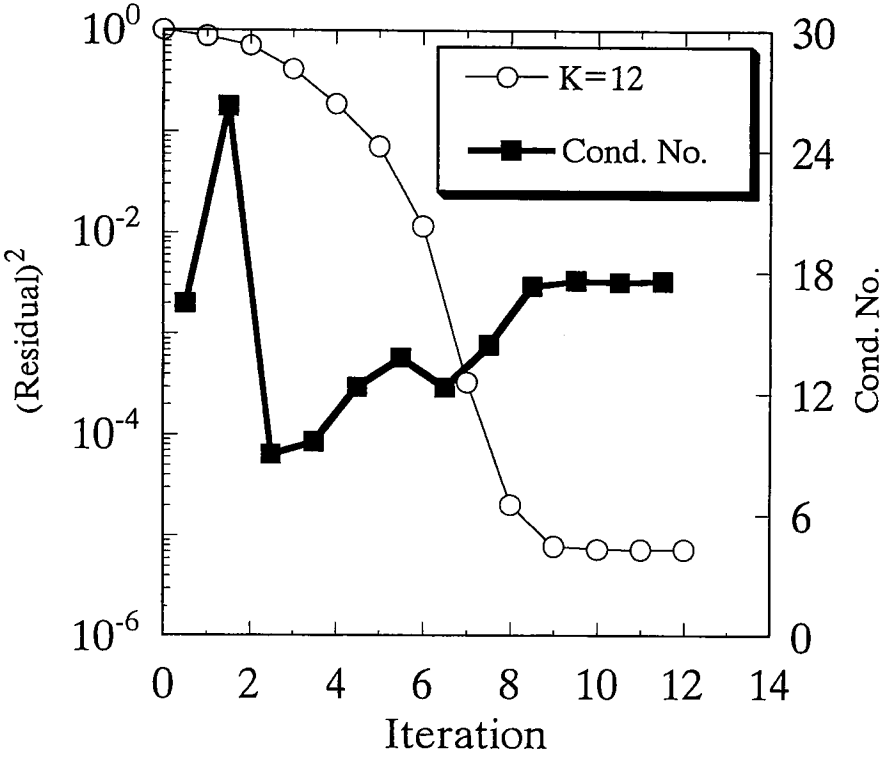
(Residual)^2
10^0
10^{-2}
10^{-4}
10^{-6}
K=12
Cond. No.
30
24
18
12
6
0
Cond. No.
0 2 4 6 8 10 12 14
Iteration

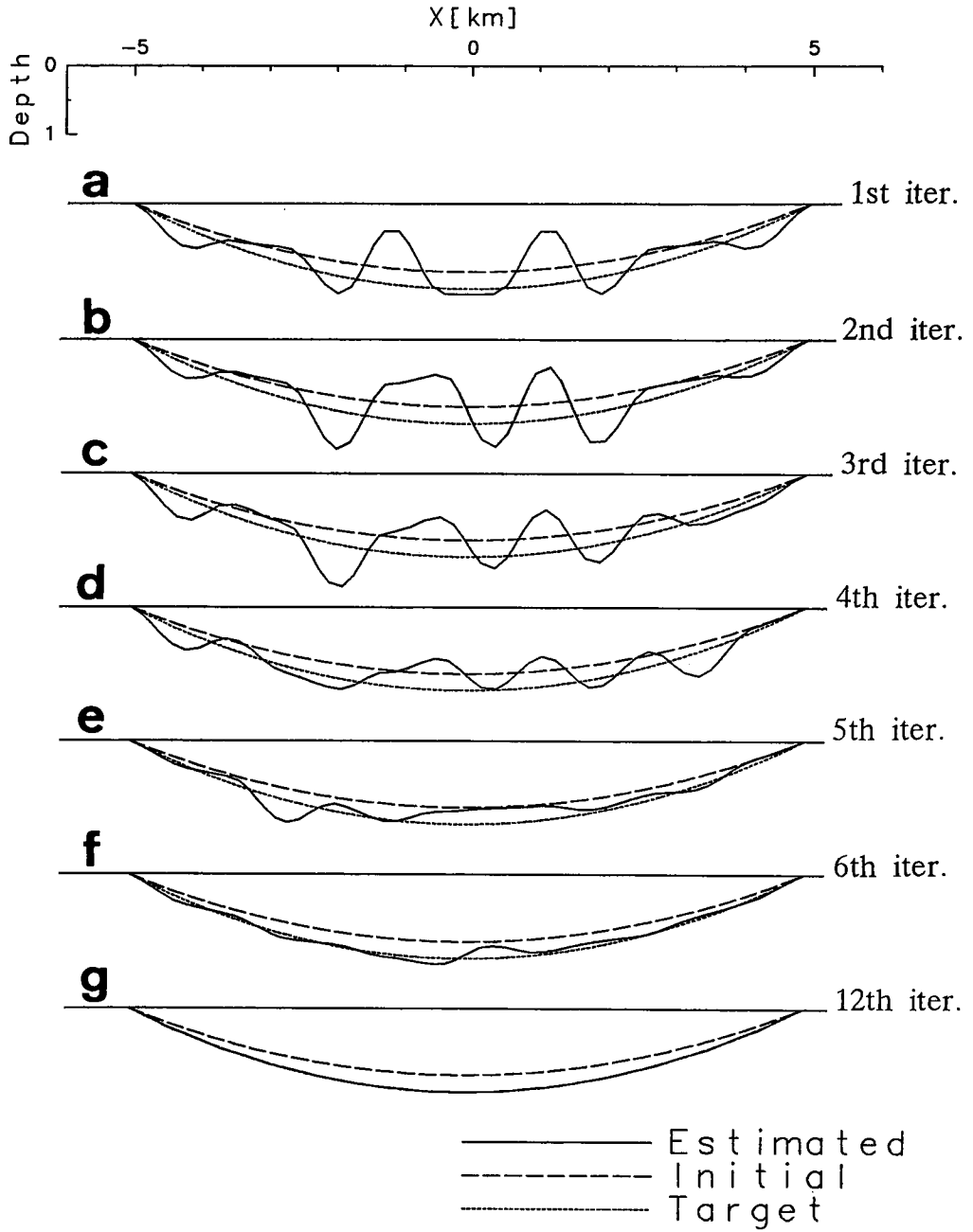
X [km]
−5
0
5
Depth
0
1
a
1st iter.
b
2nd iter.
c
3rd iter.
d
4th iter.
e
5th iter.
f
6th iter.
g
12th iter.
Estimated
Initial
Target

Fig. 13

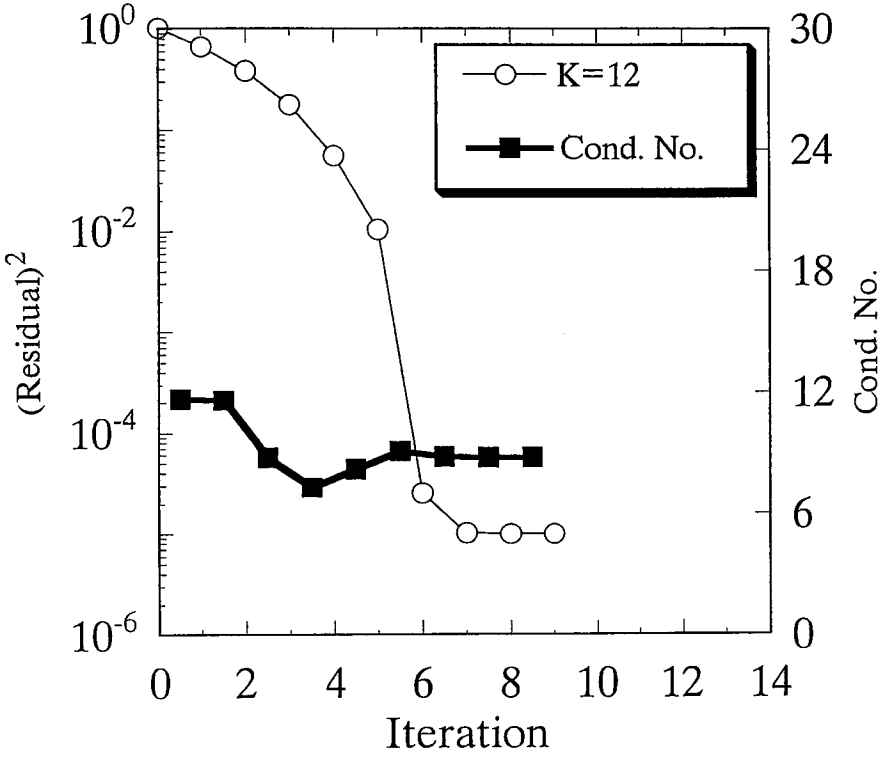
K=12
Cond. No.
(Residual)^2
Cond. No.
Iteration
10^0
10^{-2}
10^{-4}
10^{-6}
30
24
18
12
6
0
0 2 4 6 8 10 12 14

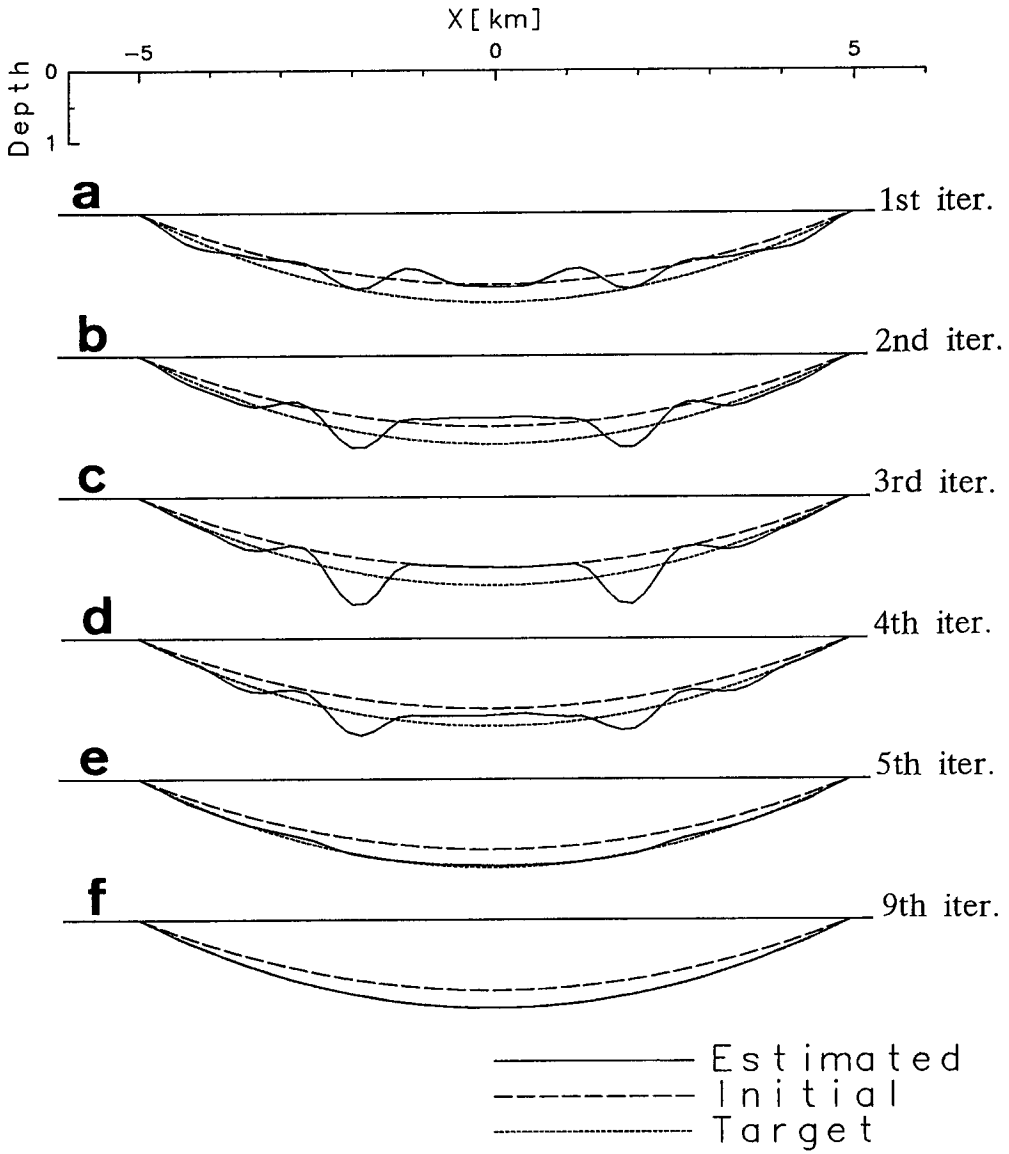
X [km]
−5
0
5
Depth
0
1
a
1st iter.
b
2nd iter.
c
3rd iter.
d
4th iter.
e
5th iter.
f
9th iter.
Estimated
Initial
Target

Fig. 14